Topological features of large fluctuations to the interior of a limit cycle

V. N. Smelyanskiy,[1] M. I. Dykman,[1] and R. S. Maier[2]
[1]*Department of Physics and Astronomy, Michigan State University, East Lansing, Michigan 48824*
[2]*Department of Mathematics, University of Arizona, Tucson, Arizona 85721*
(Received 29 October 1996)

We investigate the pattern of optimal paths along which a dynamical system driven by weak noise moves, with overwhelming probability, when it fluctuates far away from a stable state. Our emphasis is on systems that perform self-sustained periodic vibrations, and have an unstable focus inside a stable limit cycle. We show that in the vicinity of the unstable focus, the flow field of optimal paths generically displays a pattern of singularities. In particular, it contains a *switching line* that separates areas to which the system arrives along optimal paths of topologically different types. The switching line spirals into the focus and has a self-similar structure. Depending on the behavior of the system near the focus, it may be smooth, or have finite-length branches. Our results are based on an analysis of the topology of the Lagrangian manifold for an auxiliary, purely dynamical, problem that determines the optimal paths. We illustrate our theory by studying, both theoretically and numerically, a van der Pol oscillator driven by weak white noise. [S1063-651X(97)02703-7]

PACS number(s): 05.40.+j, 02.50.−r, 05.20.−y, 02.40.−k

I. INTRODUCTION

Many nonlinear dissipative systems display stable periodic oscillations, i.e., their state spaces contain stable limit cycles [1]. Examples include lasers [2], radiofrequency generators [1(a)], chemical [3(a)] and biological [3(b)] systems. In many cases the vibrations are nonsinusoidal, as in a multimode laser with strong mode coupling [4], passive optically bistable elements [5], and various sorts of engineering structure [6].

Fluctuations in periodically oscillating systems play an extremely important role. They eventually destroy periodicity of the self-sustained oscillations, so that the oscillation phase becomes random, and a stationary probability distribution in the state space of the system is formed [7,8]. This distribution reaches a maximum at the cycle, does not vary much along the cycle, and falls off rapidly in directions transverse to the cycle. The shape of the maximum depends on the character of small transverse fluctuations away from the cycle. If the fluctuations are due to the system being perturbed by weak noise (of intensity D), the transverse falloff will usually be approximately Gaussian [7–9], with standard deviation proportional to $D^{1/2}$ as $D\rightarrow 0$.

It was recognized long ago [7,10] that, for systems with stable limit cycles, it is of considerable interest to analyze the way in which *large*, occasional fluctuations away from the cycle take place. These fluctuations are responsible, e.g., for switching between coexisting laser modes [11–13], or between different photon occupation numbers of a single maser mode, as observed recently in Ref. [14]. Another interesting effect attributed to large fluctuations is a sudden transient dropout in the intensity of a main mode due to power exchange between main- and submodes [13(a)]. Recent interest in this problem is due to the application of lasers in optical communication [15].

The analysis of large fluctuations and switching between attractors, in systems with limit cycles, is similar in many ways to the analysis of the corresponding phenomena in other types of nonequilibrium system. Previous work on this is due to many authors (see Refs. [16–20] and the more recent Refs. [21–32]). In spite of much effort a full analysis of these phenomena, in systems with stable limit cycles, has been obtained only close to a bifurcation point in parameter space, where the phase and amplitude of the oscillations of the system fluctuate independently [7,8]. Corrections to the stationary probability density distribution due to weak coupling between angular and radial fluctuations are discussed in Ref. [17].

Large fluctuations in systems with stable limit cycles have several novel features, arising from the fact that there is often an unstable fixed point inside the cycle. For example, in the simplest case of a single-mode laser such a point corresponds to the unstable stationary state where the system does not generate light. If present, an unstable fixed point will be an unstable focus or node (or perhaps a saddle point if the system has more than two dynamical variables). The stationary probability density near the unstable fixed point is ''built up'' by large fluctuations away from the limit cycle. The possibility of singularities occurring, as $D\rightarrow 0$, in the probability distribution of systems lacking detailed balance was first pointed out by Graham and Tél [21] (see also Jauslin [22]). We shall show that in oscillating systems with such an unstable fixed point, the way in which fluctuations to its vicinity take place gives rise to a highly unusual *singularity structure* of the stationary probability density there (in the limit of low noise intensity D).

From one point of view, singularities arise for the following reason. The stationary probability density in the immediate vicinity of the limit cycle is determined by the dynamics of the system near the cycle, and is asymptotically Gaussian. Normally one would expect, by linearizing the motion of the system near the unstable fixed point contained within the limit cycle, that the probability density there would be an inverted Gaussian. The shape of this inverted Gaussian would be determined by the local (linearized) dynamics of the system. But it is by no means clear that two locally defined functions (a Gaussian and an inverted Gaussian) will match together smoothly. In fact, we shall see that the naive

assumption of an inverted Gaussian distribution near the unstable fixed point is incorrect.

Our approach to the problem of large fluctuations to the vicinity of an unstable fixed point makes heavy use of the *optimal path* concept. At least in the case of linear models, the concept can be traced back to the work of Onsager and Machlup [33]. An optimal path (sometimes called an Onsager-Machlup optimal path) is a path along which a dynamical system experiencing weak random perturbations moves, with overwhelming probability, when it eventually fluctuates away from the vicinity of an attractor to a specified remote point in its state space. This path provides a minimum to a certain action functional that describes the probabilities of arrival to the specified point along different paths. Each such probability becomes exponentially small as $D\rightarrow 0$, but the exponential falloff rate is path dependent, so that it becomes exponentially more probable for the system to move along a distinguished ''optimal'' trajectory than along other trajectories. The particular form of the action functional depends on the nature of the random perturbations (fluctuations may be induced by external noise, or by the number of molecules in a chemical system being finite, etc.). We emphasize that optimal paths are real physical objects: they have been experimentally observed [26]. Note that *extreme* paths, which provide extrema of the action functional, may not necessarily provide the absolute minimum. In this paper we shall study the singular properties of the flow field of extreme paths, both optimal and nonoptimal.

From a formal point of view, the analysis of a $D\rightarrow 0$ limit in terms of optimal trajectories is similar to the analysis of the $\hbar\rightarrow 0$ limit of quantum mechanics in terms of the extreme trajectories of semiclassical WKB theory. A well known feature of the pattern of extreme trajectories appearing in the semiclassical approximation is the presence of *caustics*: curves that are envelopes of trajectories, in the sense that trajectories are reflected from them [34,35]. Caustics have in fact been discovered numerically in the flow field of extreme paths of fluctuating systems of various types [22,27,29,31], [23(a)]. However, unlike a wave function in quantum mechanics, the probability density in the theory of large fluctuations, the asymptotic properties of which are determined by the flow of optimal paths, is non-negative definite. Normally a semiclassical approximation to a wave function acquires a phase factor when the WKB trajectory from which it is computed encounters a caustic. This suggests that in the asymptotic theory of fluctuating systems, *optimal* extreme trajectories are forbidden, by a sort of ''censorship,'' from ever encountering caustics. By the time they reach them, they have ceased to be optimal. This is a key difference between the $D\rightarrow 0$ limit of fluctuation theory and the $\hbar\rightarrow 0$ limit of quantum mechanics.

A topological analysis showing exactly how, in white-noise driven systems, optimal paths automatically avoid caustics was given in Ref. [30]. The analysis there was limited to fluctuations in systems whose state spaces contain only stable fixed points and saddle points; no other singularities, such as limit cycles, were discussed. For models in this restricted class, it was shown that caustics can emanate, in pairs, from *cusp points*. The location of cusp points, in the system state space, is determined by the global pattern of optimal paths; only occasionally can the location of cusp points, and caustics, be determined analytically [24(b)], [29].

In the present paper we extend and generalize the analysis of Ref. [30] to any system with a stable limit cycle that contains an unstable fixed point. In particular, we consider the case when the unstable fixed point is an unstable focus (so that in the absence of fluctuations, trajectories in the system state space spiral away from it). We shall show that generically, the flow field of optimal paths near the unstable focus displays a self-similar *pattern of singularities* (including a caustic, and under some circumstances an infinite sequence of cusps). The caustic is unobservable in the sense that optimal extreme paths are not incident on it. But the pattern is accompanied by a self-similar *switching line*: a curve that separates regions in state space that are reached via topologically different sorts of optimal path, in the weak-noise ($D\rightarrow 0$) limit. This curve spirals into the unstable focus, and its presence is responsible for the singular behavior there (in the weak-noise limit) of the stationary probability distribution.

In Sec. II we derive Hamilton's equations of motion for the extreme paths (in particular, for optimal paths), and find initial conditions for these paths in the vicinity of the stable limit cycle. In Sec. III we explain what topological singularities of the pattern of extreme paths can be like. In Sec. IV we study the behavior of the extreme paths that extend to the vicinity of the unstable focus, by linearizing Hamilton's equations of motion there. We show that generically, there is a caustic that spirals down to the unstable focus, and begin the task of determining the location of this caustic and its associated cusp points, if any. In Sec. V, by reducing the equations for the extreme paths near an unstable fixed point to a ''normal form'' (a set of uncoupled lower-order equations), we identify the parameters that determine the local dynamics of the paths. In Sec. VI we obtain explicit equations for the positions of the extreme paths, and the caustic, near the unstable focus. A detailed topological analysis of the so-called *Lagrangian manifold* formed by the paths is given, and features of the flow field of paths related to the singular structure of manifold are discussed. We also discuss the switching line. In Sec. VII the results of Sec. VI are extended to the more difficult case when the caustic spiraling down to the unstable focus has an infinite sequence of cusp points lying along it. In Sec. VIII we investigate numerically the global pattern of extreme paths for a van der Pol oscillator, and analyze global and local singularities of this pattern. Section IX contains concluding remarks.

II. EQUATIONS FOR THE EXTREME PATHS OF A FLUCTUATING SYSTEM

A. The eikonal approximation

For any dynamical system, a detailed picture of the fluctuations about an attractor, and the shape of the steady-state probability distribution, requires a specification of the underlying dynamics and the source of the fluctuations. However, the above-mentioned singular features of the distribution and of the pattern of optimal paths occur very generally. Therefore we shall consider the simplest model of a fluctuating system that can display these features: a two-variable dynamical system driven by white noise, with a stable limit

cycle containing an unstable focus or node. The equation of motion of such a system is of the form

$$\frac{d\boldsymbol{q}}{dt}=\boldsymbol{K}(\boldsymbol{q})+\boldsymbol{f}(t), \tag{1}$$

with $\langle \boldsymbol{f}(t)\rangle=\boldsymbol{0}$ and

$$\langle f_i(t)f_j(t')\rangle=DQ_{ij}\delta(t-t'), \quad i,j=1,2. \tag{2}$$

Here $\boldsymbol{q}=(q_1,q_2)$ is a vector of dynamical variables, and $\boldsymbol{f}(t)$ is white Gaussian noise with intensity D [the matrix Q_{ij} is non-negative definite, and we assume that $\max|Q_{ij}|=O(1)$]. The drift field $\boldsymbol{K}$ specifies the dynamics of the system in the absence of noise. We choose it so that the system has a limit cycle, i.e., the equation $d\boldsymbol{q}/dt=\boldsymbol{K}(\boldsymbol{q})$ has a solution $\boldsymbol{q}^{(cl)}(t)$ satisfying $\boldsymbol{q}^{(cl)}(t+\tau^{(cl)})=\boldsymbol{q}^{(cl)}(t)$, where $\tau^{(cl)}$ is the period of oscillation.

A noise-driven van der Pol oscillator [7], for example, fits into this framework. In dimensionless variables the equation of motion of such an oscillator is

$$\ddot{x}+2\eta(x^2-1)\dot{x}+x=f_1(t) \tag{3}$$

(where $\eta>0$). If one lets $q_1=x$ and $q_2=\dot{x}$, and sets

$$K_1=q_2, \quad K_2=-q_1-2\eta q_2(q_1^2-1), \quad Q_{ij}=4\eta\delta_{i2}\delta_{j2}, \tag{4}$$

then Eq. (1) reduces to Eq. (3). Notice that $\boldsymbol{q}=\boldsymbol{0}$ is an unstable fixed point of the van der Pol oscillator; it is contained within a stable limit cycle. We have $\boldsymbol{K}(\boldsymbol{0})=\boldsymbol{0}$, and

$$\det(\partial K_i/\partial q_j)_{=\boldsymbol{0}}>0, \quad (\partial K_i/\partial q_i)_{=\boldsymbol{0}}>0 \tag{5}$$

(summation over repeated indices is understood).

The stationary probability density $P=P(\boldsymbol{q})$ of any system described by Eqs. (1) and (2) satisfies the time-independent Fokker-Planck equation

$$\frac{D}{2}\frac{\partial^2}{\partial q_i\partial q_j}[Q_{ij}P(\boldsymbol{q})]-\frac{\partial}{\partial q_i}[K_iP(\boldsymbol{q})]=0. \tag{6}$$

In the limit of small noise intensity D one can seek an approximate solution of Eq. (6) in an eikonal or WKB form [36]

$$P(\boldsymbol{q})\sim C(\boldsymbol{q})\exp[-S(\boldsymbol{q})/D], \quad D\to 0. \tag{7}$$

Equation (7) is a sort of asymptotic Maxwell-Boltzmann distribution, with $S(\boldsymbol{q})$ the ''activation energy'' of fluctuations to the vicinity of the point $\boldsymbol{q}$ in the system state space. $C(\boldsymbol{q})$ is a WKB prefactor, which we shall not investigate in any detail in this paper. If one substitutes the asymptotic form (7) into Eq. (6), and keeps only the terms of lowest order in D, one arrives at the following nonlinear partial differential equation for the function $S(\boldsymbol{q})$:

$$H(\boldsymbol{q},\boldsymbol{p})\equiv\boldsymbol{K}(\boldsymbol{q})\cdot\boldsymbol{p}+\tfrac{1}{2}\boldsymbol{p}\hat{\boldsymbol{Q}}\boldsymbol{p}=0, \quad \boldsymbol{p}\equiv\frac{\partial S}{\partial\boldsymbol{q}}. \tag{8}$$

Here the matrix operator $\hat{\boldsymbol{Q}}$ corresponds to the diffusion matrix Q_{ij} in Eq. (6). Equation (8) can be interpreted as the Hamilton-Jacobi equation of an *auxiliary Hamiltonian dynamical system*, with the Hamiltonian $H(\boldsymbol{q},\boldsymbol{p})$. In this interpretation $S(\boldsymbol{q})$ is a *classical action at zero energy*.

If the noise is weak, the probability density $P(\boldsymbol{q})$ will be tightly peaked around the stable limit cycle. Moreover because of phase diffusion [7], the function $S(\boldsymbol{q})$ should be constant on the limit cycle to leading order in D as $D\to 0$. It follows [21(b)] that $S(\boldsymbol{q})$ satisfies the following boundary conditions on the limit cycle:

$$\left(\frac{\partial S}{\partial\boldsymbol{q}}\right)_{\mathbf{q}=\boldsymbol{q}^{(cl)}(\tau)}=0, \quad S(\boldsymbol{q}^{(cl)}(\tau))=\text{ const}, \tag{9}$$

for all $\tau\in(0,\tau^{(\mathrm{cl})})$. Here τ has the meaning of elapsed time for deterministic motion along the limit cycle.

The Hamilton-Jacobi equation (8) may be solved by the method of characteristics. The equations for the characteristics have the form

$$\frac{d\boldsymbol{q}}{dt}=\frac{\partial H}{\partial\boldsymbol{p}}=\boldsymbol{K}(\boldsymbol{q})+\hat{\boldsymbol{Q}}\boldsymbol{p}, \tag{10a}$$

$$\frac{d\boldsymbol{p}}{dt}=-\frac{\partial H}{\partial\boldsymbol{q}}=-\frac{\partial\boldsymbol{K}(\boldsymbol{q})}{\partial\boldsymbol{q}}\boldsymbol{p}, \tag{10b}$$

and the evolution equation for S along any characteristic is

$$\frac{dS}{dt}=\boldsymbol{p}\cdot\dot{\boldsymbol{q}}. \tag{11}$$

Equations (10) are Hamilton's equations of motion for the auxiliary system. They describe the trajectories of this system that give rise to extreme values of its action functional [37,38]. This action functional is of the form

$$\mathcal{S}[\boldsymbol{q}(t)]=\int_{t_{\min}}^{t_{\max}}[\dot{\boldsymbol{q}}(t)-\boldsymbol{K}(\boldsymbol{q}(t))]\hat{\boldsymbol{Q}}^{-1}[\dot{\boldsymbol{q}}(t)-\boldsymbol{K}(\boldsymbol{q}(t))]dt.$$

In general there will be many zero-energy trajectories that begin on the stable limit cycle and terminate at a specified point $\boldsymbol{q}'$. As a consequence, the quantity $S(\boldsymbol{q}')$ is in general *multivalued*. One of these trajectories gives the *least* action. This least value $S_{\min}(\boldsymbol{q}')$ is the physical value of the zero-energy action: the one that would appear in the eikonal approximation (7) to the stationary probability density P at the point $\boldsymbol{q}'$.

Using a path-integral formulation of the problem of large fluctuations [20,26], [24(b)], or an equivalent probabilistic formalism [16], one can show that the extreme trajectory $\boldsymbol{q}(t)$ giving rise to $S_{\min}(\boldsymbol{q}')$ is the *optimal fluctuational trajectory* of the original dynamical system that reaches $\boldsymbol{q}'$. When a fluctuation to the vicinity of any point $\boldsymbol{q}'$ not on the limit cycle occurs, in the $D\to 0$ limit it becomes increasingly likely that the fluctuation took place along the optimal trajectory. The optimal trajectory of the system corresponds to an optimal (most probable) realization of the random force $\boldsymbol{f}$.

The auxiliary dynamical system, being Hamiltonian, has dynamical variables $(\boldsymbol{q},\boldsymbol{p})$. What is the significance of the momentum $\boldsymbol{p}$ for the original noise-perturbed dynamical system? Through the eikonal approximation, at any point $\boldsymbol{q}$

along an optimal path the momentum $\boldsymbol{p}$ determines the $D\to 0$ limit of the logarithmic gradient of the stationary probability density. Moreover, the momentum may be interpreted as a measure of the extent to which optimal trajectories move against the deterministic drift $\boldsymbol{K}$. It is clear from Hamilton's equation (10a) that $\boldsymbol{p}=\boldsymbol{0}$ only for trajectories satisfying $\dot{\boldsymbol{q}}=\boldsymbol{K}(\boldsymbol{q})$, i.e., deterministic (nonfluctuational) trajectories.

B. Initial conditions for extreme trajectories

The initial conditions for the extreme trajectories emanating from the stable limit cycle, i.e., the zero-energy trajectories satisfying Eq. (10), follow from the behavior of the classical action function $S(\boldsymbol{q})$ in the vicinity of the cycle. Because the gradient $\nabla S(\boldsymbol{q})$ vanishes on the cycle, near the cycle one may seek an *approximately quadratic* solution for the action, of the sort first considered by Ludwig [18] (cf. Refs. [9,25])

$$S(\xi_l,\xi_n)\approx \tfrac{1}{2}\lambda(\xi_l)\xi_n^2. \tag{12}$$

The coordinate ξ_l is the distance along the limit cycle (measured from an arbitrary point). The other coordinate, ξ_n, is the normal distance to the limit cycle. In the limit of small noise intensity we have what is effectively one-dimensional diffusion normal to the limit cycle, and Eqs. (7) and (12) describe the Gaussian distribution of the system in that direction.

The equation for ξ_l as a function of the time τ of motion along the cycle has the form $d\xi_l/d\tau=v_l(\tau)$, where $v_l(\tau)$ is the speed along the cycle. One can view λ in Eq. (12) as a function of the time variable τ, rather than ξ_l. A Riccati equation for $\bar{\lambda}(\tau)\equiv\lambda[\xi_l(\tau)]$ can be obtained by substituting Eq. (12) into the zero-energy Hamilton-Jacobi equation (8) and taking the limit $\xi_n\to 0$. It has the form [25]

$$\dot{\bar{\lambda}}+2\frac{\partial v_n}{\partial\xi_n}\bar{\lambda}+Q_{nn}\bar{\lambda}^2=0,\quad \bar{\lambda}(\tau+\tau^{(cl)})=\bar{\lambda}(\tau), \tag{13}$$

$$v_n\equiv\boldsymbol{K}\cdot\hat{\boldsymbol{\xi}}_n,\quad Q_{nn}\equiv\hat{\boldsymbol{\xi}}_n\hat{\boldsymbol{Q}}\hat{\boldsymbol{\xi}}_n.$$

Here $\hat{\boldsymbol{\xi}}_l$ and $\hat{\boldsymbol{\xi}}_n$ are orthogonal unit vectors that are locally parallel and perpendicular to the limit cycle. So v_n is the component of the velocity $\boldsymbol{K}$ normal to the cycle, and DQ_{nn} is the diffusion coefficient in the direction normal to the cycle (clearly $v_n=0$ on the cycle, i.e., at $\xi_n=0$). The coefficients $\partial v_n/\partial\xi_n$ and Q_{nn} are evaluated on the cycle. They depend on the position along the cycle ξ_l, or, equivalently, on the time τ. This dependence is periodic, and the solution $\bar{\lambda}=\bar{\lambda}(\tau)$ should be periodic as well, which uniquely determines it. Eq. (13) can be reduced to a linear equation for the function $1/\bar{\lambda}(\tau)$ and then solved, yielding an explicit approximation to the action $S(\boldsymbol{q})$ near the limit cycle [9,25].

Since $\boldsymbol{p}=\nabla S$, Eq. (12) yields the following expressions for the components of the momentum $\boldsymbol{p}$ parallel to and perpendicular to the cycle

$$p_l(\xi_l,\xi_n)\approx\frac{1}{2}\frac{d\lambda}{d\xi_l}\xi_n^2,\quad p_n(\xi_l,\xi_n)\approx\lambda(\xi_l)\xi_n, \tag{14}$$

when $|\xi_n|\ll 1$. In what follows we shall set $p_l\approx 0$, because p_l is of the same order of magnitude as the terms in the equation for p_n that arise from the cubic-in-ξ_n corrections to the action that were dropped in Eq. (12). The smallness of p_l as compared to p_n has the following explanation. In contrast to the deterministic trajectories of the system in the absence of noise, the extreme trajectories near the limit cycle spiral *away* from the cycle; however, the direction of spiraling is the same. Deterministic trajectories satisfy equations of the form (10), with $\boldsymbol{p}=\boldsymbol{0}$, and therefore it is clear that p_l is small compared to p_n near the cycle.

It follows from Eqs. (14) that the initial conditions for zero-energy extreme trajectories emanating from the limit cycle can be chosen in the following way. Suppose that at an initial instant t_0 we choose $\boldsymbol{q}(t_0)$ to be close to the limit cycle. We may then set

$$\boldsymbol{p}(t_0)=\lambda(\xi_l)\xi_n\hat{\boldsymbol{\xi}}_n,\quad S(t_0)=\tfrac{1}{2}\lambda(\xi_l)\xi_n^2, \tag{15}$$

where $\xi_l\equiv\xi_l(\boldsymbol{q}(t_0))$ and $\xi_n\equiv\xi_n(\boldsymbol{q}(t_0))$. Since the zero-energy trajectories satisfying Eq. (10) spiral away from the cycle, it is clear that we shall describe one and the same path if the value of $\xi_n(\boldsymbol{q}(t_0))$ differs by the increment of ξ_n over one turn (or over several turns). The entire flow of the zero-energy Hamiltonian trajectories emanating from the limit cycle is therefore mapped onto the two intervals of ξ_n (one for positive and one for negative ξ_n) that lie between the neighboring turns of a single path. In other words, the entire family of zero-energy extreme trajectories emanating from the limit cycle can be parameterized as $\boldsymbol{q}(t;\xi_n)$, $\boldsymbol{p}(t;\xi_n)$, with ξ_n lying within one of the corresponding intervals, which depend on the choice of ξ_l. This fact paves the way to a numerical analysis of the global flow. The numerical analysis of a particular system (the van der Pol oscillator mentioned in Sec. II A), using this technique, will be given in Sec. VIII.

III. SINGULARITIES OF THE PATTERN OF OPTIMAL PATHS

A. Many valuedness and the generation of singularities

A well known property of Hamiltonian trajectories is that they may correspond to a local extremum rather than to the global minimum of the action functional. On account of the existence of local extrema, several extreme trajectories $\boldsymbol{q}(t,\xi_n)$ with different values of the parameter ξ_n may arrive at the same point $\boldsymbol{q}$. The action $S(t;\xi_n)$ as computed from the differential equation (11) will be, in general, a multivalued function of the end point $\boldsymbol{q}$. If at each point $\boldsymbol{q}$ one selects the minimum value of $S(\boldsymbol{q})$, then a single-valued surface of *minimum* action $S_{\min}=S_{\min}(\boldsymbol{q})$ will be defined piecewise. The quantity $S_{\min}(\boldsymbol{q})$ determines the asymptotic ($D\to 0$) logarithm of the stationary probability distribution $P=P(\boldsymbol{q})$ via the eikonal approximation Eq. (7).

Generically, the surface $S_{\min}=S_{\min}(\boldsymbol{q})$ will contain curves (''switching lines'') at which different sheets of $S=S(\boldsymbol{q})$ intersect each other transversally, i.e., at a nonzero angle. Along any such curve the first derivative of $S_{\min}(\boldsymbol{q})$ in the transverse direction will be discontinuous [21,22]. However, the resulting singularities of the distribution $P(\boldsymbol{q})$ will be smeared out at nonzero noise intensity D. They appear only asymptotically, as $D\to 0$.

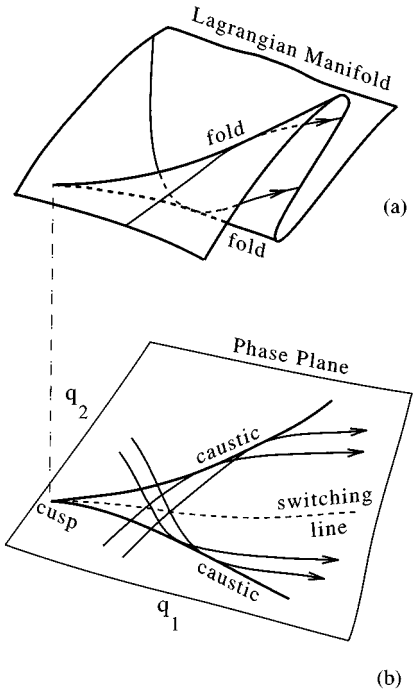

FIG. 1. Generic singularities of the pattern of extreme paths. The Lagrangian manifold (LM), a two-dimensional submanifold of the four-dimensional phase space, is traced out by the trajectories of the auxiliary Hamiltonian system that emanate from the limit cycle. Extreme paths are the projections of these trajectories onto the (q_1,q_2) plane (i.e., the $\boldsymbol{p}=\mathbf{0}$ plane). The LM may have folds, in which case the projections of these folds are caustics, from which extreme paths are reflected. In the region enclosed by a pair of caustics and sufficiently close to the cusp from which they emanate, three extreme paths pass through each point (q_1,q_2).

Singularities may also appear on individual branches of the multivalued function $S(\boldsymbol{q})$. To investigate these singularities, and related singular features of the pattern of extreme trajectories, one needs to study the generic topological properties of the auxiliary Hamiltonian system in its four-dimensional phase space. It follows from Hamilton's equations (10) that in this space, a stable limit cycle in configuration space (determined by the drift field $\boldsymbol{K}$) corresponds to a closed loop on the hyperplane $\boldsymbol{p}=\mathbf{0}$. [This hyperplane is just the two-dimensional plane (q_1,q_2) of the original dynamical system.] The zero-energy Hamiltonian trajectories determined by Eq. (10) emanate from this limit set and form a two-dimensional *Lagrangian manifold* (LM) [1(b)], [40]. The LM lies in the zero-energy $(H=0)$ surface, which is three dimensional. The LM is a sort of *ruled surface*: the zero-energy Hamiltonian trajectories, i.e., extreme trajectories, provide a smooth flow on it.

Even though the extreme trajectories never intersect on the LM, except at the loop on the $\boldsymbol{p}=\mathbf{0}$ plane from which they emerge, the LM may have a complicated structure. In general, it will have [40] singular projections onto the $\boldsymbol{p}=\mathbf{0}$ plane, i.e., the (q_1,q_2) plane. A two-dimensional LM has only two structurally stable types of singularities [39]: *folds* and *cusps*, as illustrated in Fig. 1. Each cusp point gives rise to a pair of folds, and in the case of monostable systems the folds can only begin or end at a cusp point or at infinity. The projections of the folds onto the $\boldsymbol{q}$ plane are caustics. Caustics are *envelopes of trajectories*: they are formed by intersecting neighboring trajectories $\boldsymbol{q}=\boldsymbol{q}(t)$. It is from the merging of caustics that cusp points are formed (see Fig. 1). In the event that the LM contains a fold, the top and bottom sheets of the LM are traced out by Hamiltonian trajectories that have not gone over the fold. After a trajectory goes over a fold, it enters the middle sheet of the LM and stays there.

In the sharp-tipped triangular region partially enclosed by caustics, the LM has three sheets and the action is three valued. It was observed in Ref. [30] that the sheet with the largest value of $S(\boldsymbol{q})$ is the middle sheet of the LM. This sheet is formed by Hamiltonian trajectories that have gone over the fold; equivalently, the corresponding extreme trajectories in the $\boldsymbol{q}$ plane have been ''reflected'' by one of the caustics. So the minimum (physical) value of $S(\boldsymbol{q})$, i.e., $S_{\min}(\boldsymbol{q})$, must be attained on one of the other two sheets, which we may call the ''lower'' sheets. We provide a careful proof of this fact in the Appendix.

The nonminimality of the action computed from the trajectories reflected from a caustic is a most important feature of the topological theory of large fluctuations. It guarantees that *optimal* extreme trajectories never encounter caustics: by the time an optimal trajectory is reflected from a caustic, it has ceased to be optimal. Indeed, the two lower sheets of the action surface $S=S(\boldsymbol{q})$ must intersect, and by the time either of these sheets approaches the fold (where it turns over, and merges with the sheet formed by the trajectories reflected from the caustic), it has intersected the other lower sheet and necessarily lies above it.

The curve in the (q_1,q_2) plane along which the lower sheets intersect is determined by the equation

$$S^{(1)}(q_1,q_2)=S^{(2)}(q_1,q_2). \tag{16}$$

This curve starts at the cusp point and lies between the coalescing caustics [Fig. 1(b)]. Points that are a small distance away from the curve (16), but lie on opposite sides of it, are reached along topologically different optimal paths (those tracing out the two lower sheets). It is for this reason that we call the curve determined by Eq. (16) a switching line. Switching lines can be observed using a technique [26] where one investigates the probability distribution of paths $\boldsymbol{q}(t)$ along which the system arrives at a specified end point $\boldsymbol{q}'$. If this distribution is measured for various positions of $\boldsymbol{q}'$, its shape will change sharply once $\boldsymbol{q}'$ is moved across a switching line. This is the physical significance of the singular curves in the surface $S_{\min}=S_{\min}(\boldsymbol{q})$ of the system.

The stationary probability density is regular in the vicinity of a switching line. In the event of multivaluedness, the WKB approximation (7) may be refined to read

$$P(\boldsymbol{q})\sim\sum_{i=1,2}C^{(i)}(\boldsymbol{q})\exp[-S^{(i)}(\boldsymbol{q})/D],\quad D\to 0 \tag{17}$$

(cf. [21(b)], [30,35]). A switching line is, therefore, a sort of *Stokes line*, where asymptotic dominance switches from one exponential term to another. We note in passing that the WKB prefactors $C^{(i)}(\boldsymbol{q})$ are not singular on switching lines. They do, however, blow up when $\boldsymbol{q}$ approaches a cusp point.

An explicit form for the prefactor in the vicinity of a cusp point was obtained in Ref. [30] (see also the scaling theory of Ref. [41]).

We emphasize that the caustics of a flow field of extreme paths, unlike its switching lines, are unobservable. They are hidden: as one varies the endpoint $\boldsymbol{q}'$, switching from one optimal path to another occurs before the optimal path terminating at $\boldsymbol{q}'$ encounters a caustic *en route*. (In contrast to the $D\to 0$ limit of large fluctuation theory, caustics *are* encountered by the extreme paths occurring in the $\hbar\to 0$ limit of quantum mechanics.)

Topological arguments explain *how* caustics are avoided by optimal paths, and what are the observable singularities (switching lines and cusp points) of the pattern of optimal paths. In general, two different types of pattern may occur near a cusp point. One of them corresponds to the local picture shown in Fig. 1(b). In that figure the caustics go ''away from'' the cusp point rather than ''towards'' it (the direction of a caustic, in our convention, is the direction of the extreme trajectories to which the caustic is tangent). Extreme trajectories that come from opposite sides of the cusp point first cross each other and only then encounter caustics (the paths are observable, i.e., physically significant, up to the point of their intersection). However, the flow of the trajectories near the cusp may also be in the opposite direction, i.e., the caustics may go towards the cusp point, in which case the extreme paths first encounter caustics (after which time they become nonoptimal, i.e., unobservable) and then cross each other. In what follows we shall refer to the two types of cusp points as type-I and type-II, respectively.

Clearly, there is no switching line emanating from a type-II cusp point. Unlike the type-I cusp points, the type-II cusp points are *hidden singularities*. They lie on nonminimal sheets of the action surface $S=S(\boldsymbol{q})$.

It can be seen from the preceding arguments that a switching line may not connect two cusp points. However two switching lines emanating from different cusp points may end in a point where they intersect each other, with another switching line starting at this point. In this way there may arise physically observable *trees of switching lines*, with the ''free'' ends of the lines (i.e., the leaves of the tree) located at observable cusp points. In Sec. VIIB we shall illustrate this with an example.

B. Monostable systems vs systems with unstable stationary states

In any monostable noise-driven dynamical system, on physical grounds one expects that it is possible to reach any point (q_1,q_2) by traversing a smooth optimal path which emanates from the attractor and avoids all singularities. The flow field of extreme paths, both optimal and nonoptimal, may include caustics. But optimal paths avoid them. The flow field of optimal paths is qualitatively different in the case when the dynamical system, in the absence of noise, has unstable stationary states. Since unstable fixed points are critical points of the deterministic dynamics, they are singular points of the flow field of optimal paths as well.

In the following sections we shall investigate the occurrence of various singular features in the vicinity of an unstable fixed point, contained within a stable limit cycle. We shall show that, except in the trivial case when radial and angular fluctuations are independent of each other, the structure of the pattern of optimal paths is quite singular when the unstable fixed point is an unstable focus (the case when it is an unstable node will be considered elsewhere). This structure can be fully investigated analytically.

A key role in our analysis will be played by the *most probable hitting path* (MPHP). This is the optimal path along which the system moves from the stable limit cycle to the unstable fixed point. That is, in the limit of weak noise $(D\to 0)$, it becomes overwhelmingly likely that a large fluctuation from the limit cycle to the unstable fixed point, when it finally occurs, will follow this path. Generically, there can be only one MPHP: the action for reaching the unstable fixed point along different extreme paths that might ''hit'' the fixed point is different, and for the MPHP it must be a minimum. The MPHP is a *heteroclinic trajectory* of the associated Hamiltonian dynamical system in its four-dimensional phase space: it lies both in the unstable manifold of the stable limit cycle, and in the stable manifold of the unstable fixed point. Optimal paths close to the MPHP, but lying on opposite sides of it, will diverge from the MPHP in the vicinity of the unstable fixed point. As we shall see, this causes the fluctuational behavior of the dynamical system to be very singular there. From a dynamical systems point of view, it is *wild oscillations* of the Lagrangian manifold in the vicinity of the unstable fixed point (cf. Graham and Tél [21]) that give rise to the singular structure we shall explore.

IV. EXTREME PATHS IN THE VICINITY OF AN UNSTABLE FIXED POINT

A. The linear approximation

As we have discussed, the fluctuational behavior of an oscillating dynamical system is determined by the pattern of extreme paths that emanate from its stable limit cycle. In this section we analyze the behavior of these paths, when they are prolonged to the vicinity of the unstable fixed point enclosed by the limit cycle. We choose the position of the unstable fixed point to be $\boldsymbol{q}=(q_1,q_2)=(0,0)$. In this section and Sec. V, we do not specialize to the case of an unstable focus; we allow the unstable fixed point to be either a focus or a node. The drift field can be linearized at the unstable point

$$\boldsymbol{K}(\boldsymbol{q})\approx\hat{\boldsymbol{d}}\boldsymbol{q};\quad d_{ij}\equiv\left(\frac{\partial K_i}{\partial q_j}\right)_{\mathbf{q}=\mathbf{0}}. \tag{18}$$

The matrix $\hat{\boldsymbol{d}}$ may be called a matrix of drift coefficients. In the approximation (18) the Hamiltonian of the auxiliary system (8) becomes quadratic in $\boldsymbol{q}$ and $\boldsymbol{p}$

$$H(\boldsymbol{q},\boldsymbol{p})\approx\boldsymbol{p}\hat{\boldsymbol{d}}\boldsymbol{q}+\tfrac{1}{2}\boldsymbol{p}\hat{\boldsymbol{Q}}\boldsymbol{p}. \tag{19}$$

The corresponding linearized Hamilton's equations of motion for the coordinates and momenta may be written in matrix form as

$$\begin{pmatrix}\dot{\boldsymbol{q}}\\ \dot{\boldsymbol{p}}\end{pmatrix}=\hat{\boldsymbol{T}}\begin{pmatrix}\boldsymbol{q}\\ \boldsymbol{p}\end{pmatrix},\quad \hat{\boldsymbol{T}}=\begin{pmatrix}\hat{\boldsymbol{d}} & \hat{\boldsymbol{Q}}\\ 0 & -\hat{\boldsymbol{d}}^{\dagger}\end{pmatrix}. \tag{20}$$

Here $\hat{\boldsymbol{T}}$ is a 4×4 matrix. Its first two eigenvalues coincide with those of the matrix $\hat{\boldsymbol{d}}$, which we shall denote λ_1 and λ_2. These eigenvalues have positive real part, by assumption. The corresponding eigenvectors of $\hat{\boldsymbol{T}}$ have their momentum components identically equal to zero, whereas their position components are the eigenvectors $\boldsymbol{q}_{1,2}^{\mathcal{D}}$ of the matrix $\hat{\boldsymbol{d}}$. Linear combinations of these two eigenvectors,

$$\begin{pmatrix} \boldsymbol{q}^{\mathcal{D}}(t) \\ 0 \end{pmatrix} \equiv C_1^{\mathcal{D}} \begin{pmatrix} \boldsymbol{q}_1^{\mathcal{D}} \\ 0 \end{pmatrix} e^{\lambda_1 t} + C_2^{\mathcal{D}} \begin{pmatrix} \boldsymbol{q}_2^{\mathcal{D}} \\ 0 \end{pmatrix} e^{\lambda_2 t}, \tag{21}$$

describe deterministic trajectories of the system on the (q_1,q_2)-plane. [Recall that $\boldsymbol{p}=\boldsymbol{0}$ signifies a deterministic, nonfluctuational trajectory, satisfying $\dot{\boldsymbol{q}}=\boldsymbol{K}(\boldsymbol{q})$.]

The other two eigenvalues of the matrix $\hat{\boldsymbol{T}}$ coincide with those of the matrix $-\hat{\boldsymbol{d}}^{\dagger}$, and are equal to $-\lambda_1$ and λ_2. The corresponding eigenvectors $(\boldsymbol{q}_{1,2}^{\mathcal{F}},\boldsymbol{p}_{1,2}^{\mathcal{F}})$ will have both position and momentum components nonzero. Linear combinations of these two eigenvectors, of the form

$$\begin{pmatrix} \boldsymbol{q}^{\mathcal{F}}(t) \\ \boldsymbol{p}^{\mathcal{F}}(t) \end{pmatrix} \equiv C_1^{\mathcal{F}} \begin{pmatrix} \boldsymbol{q}_1^{\mathcal{F}} \\ \boldsymbol{p}_1^{\mathcal{F}} \end{pmatrix} e^{-\lambda_1 t} + C_2^{\mathcal{F}} \begin{pmatrix} \boldsymbol{q}_2^{\mathcal{F}} \\ \boldsymbol{p}_2^{\mathcal{F}} \end{pmatrix} e^{-\lambda_2 t}, \tag{22}$$

are ''purely fluctuational'' solutions of Eqs. (20). Unlike the deterministic trajectories, they approach the unstable point $\boldsymbol{q}=\boldsymbol{0}$ as $t\to\infty$. An arbitrary zero-energy Hamiltonian trajectory satisfying Eq. (20) is a mixture, or superposition, of the trajectories (21)–(22), i.e., is of the form

$$\begin{pmatrix} \boldsymbol{q}(t) \\ \boldsymbol{p}(t) \end{pmatrix} = \begin{pmatrix} \boldsymbol{q}^{\mathcal{D}}(t)+\boldsymbol{q}^{\mathcal{F}}(t) \\ \boldsymbol{p}^{\mathcal{F}}(t) \end{pmatrix}. \tag{23}$$

In dynamical systems terms, the trajectories (21) and (22) trace out the unstable and stable manifolds of the fixed point $(\boldsymbol{q},\boldsymbol{p})=(\boldsymbol{0},\boldsymbol{0})$ of the auxiliary Hamiltonian system (19) in its four-dimensional phase space (cf. [16,18,20,42]). The unstable manifold, which is formed by the deterministic trajectories, is simply the plane $\boldsymbol{p}=\boldsymbol{0}$, while the stable manifold, which is formed by the fluctuational trajectories of the form (22), is a ''canted'' plane of the form

$$\boldsymbol{p}=\hat{\boldsymbol{A}}\boldsymbol{q}, \tag{24}$$

where $\hat{\boldsymbol{A}}$ is an appropriate 2×2 matrix. The explicit form of $\hat{\boldsymbol{A}}$ will be discussed below. The form of the matrix $\hat{\boldsymbol{T}}$ of Eq. (20), and the zero-energy condition $H=0$, yield certain relations between the trajectories on the stable and unstable manifolds. In particular, since the eigenvectors $\boldsymbol{q}_{1,2}^{\mathcal{D}}$ of the matrix $\hat{\boldsymbol{d}}$ and eigenvectors $\boldsymbol{p}_{1,2}^{\mathcal{F}}$ of the matrix $-\hat{\boldsymbol{d}}^{\dagger}$ are orthogonal in the general case $\lambda_1\neq\lambda_2$, i.e.,

$$\boldsymbol{q}_i^{\mathcal{D}}\cdot\boldsymbol{p}_{3-i}^{\mathcal{F}}\equiv0, \quad i=1,2, \tag{25}$$

one can show that there is an invariant

$$\boldsymbol{q}^{\mathcal{D}}(t)\hat{\boldsymbol{A}}\boldsymbol{q}^{\mathcal{F}}(t)=\text{const}. \tag{26}$$

On the other hand, if one substitutes $\boldsymbol{q}=\boldsymbol{q}^{\mathcal{F}}+\boldsymbol{q}^{\mathcal{D}}$, $\boldsymbol{p}=\boldsymbol{p}^{\mathcal{F}}+\boldsymbol{p}^{\mathcal{D}}$ into $H(\boldsymbol{q},\boldsymbol{p})$ and notes that $H(\boldsymbol{q}^{\mathcal{F}},\boldsymbol{p}^{\mathcal{F}})\equiv0$ and $H(\boldsymbol{q}^{\mathcal{D}},\boldsymbol{p}^{\mathcal{D}})\equiv0$, and that $\hat{\boldsymbol{d}}\boldsymbol{q}^{\mathcal{D}}\equiv\dot{\boldsymbol{q}}^{\mathcal{D}}$, $\boldsymbol{p}^{\mathcal{F}}\hat{\boldsymbol{d}}\equiv-\dot{\boldsymbol{p}}^{\mathcal{F}}$, one obtains from Eqs. (24) and (25)

$$\dot{\boldsymbol{q}}^{\mathcal{D}}(t)\hat{\boldsymbol{A}}\boldsymbol{q}^{\mathcal{F}}(t)=\boldsymbol{q}^{\mathcal{D}}(t)\hat{\boldsymbol{A}}\dot{\boldsymbol{q}}^{\mathcal{F}}(t)=0. \tag{27}$$

Equations (26) and (27) can be viewed as a constraint on the sorts of superposition of deterministic and fluctuational trajectories that are allowed.

B. Caustics and cusp points

Every extreme trajectory emanating from the limit cycle, when prolonged to the vicinity of the unstable fixed point contained within it, must be a superposition of the form (23), constrained by Eqs. (26) and (27). It was shown in Sec. IIB that extreme trajectories, regarded as trajectories in the four-dimensional phase space, form a one-parameter set $t\mapsto(\boldsymbol{q}(t,\mu),\boldsymbol{p}(t,\mu))$. The parameter μ determines, in particular, the values of the coefficients $C_{1,2}^{\mathcal{F},\mathcal{D}}$ in Eqs. (21)–(23), which describe the behavior of the extreme trajectories that extend to the vicinity of the unstable stationary state $\boldsymbol{q}=\boldsymbol{0}$. In general, to find this dependence it is necessary to integrate Hamilton's equations (10) from the stable limit cycle down to the range of small $\boldsymbol{q}$. However, the singular features of the pattern of the paths in the vicinity of $\boldsymbol{q}=\boldsymbol{0}$ can be found from a local analysis. For a saddle point this was done in Ref. [30]. Here we shall generalize the technique of Ref. [30] to study the pattern of extreme paths near an unstable focus.

As mentioned in Sec. III B, we assume on physical grounds that there exists a single most probable hitting path (MPHP) along which the system preferentially fluctuates to the point $\boldsymbol{q}=\boldsymbol{0}$, in the $D\to0$ limit. As a trajectory in phase space, the MPHP is a heteroclinic trajectory along which the unstable Lagrangian manifold (LM) of the limit cycle $\boldsymbol{q}=\boldsymbol{q}^{(cl)}(t)$, $\boldsymbol{p}=\boldsymbol{0}$ and the stable manifold of the point $\boldsymbol{q}=\boldsymbol{p}=\boldsymbol{0}$ intersect each other. We normalize our parametrization of extreme paths by requiring that the MPHP be the extreme path with $\mu=0$.

The LM is traced out by the extreme trajectories $\boldsymbol{q}(t,\mu)$, $\boldsymbol{p}(t,\mu)$. The portion of the LM on which $|\mu|$ is small, i.e., the portion of the LM near the MPHP, is smooth. This implies that the coefficients $C_{1,2}^{\mathcal{F}},C_{1,2}^{\mathcal{D}}$ in Eqs. (21)–(23) for the extreme trajectories are smooth functions of μ near $\mu=0$. In other words, at any given instant of time t the values of the coefficients $C_{1,2}^{\mathcal{F}},C_{1,2}^{\mathcal{D}}$ for the extreme paths $\boldsymbol{q}(t,\mu)$, $\boldsymbol{p}(t,\mu)$, with μ small, are close to the values of $C_{1,2}^{\mathcal{F}},C_{1,2}^{\mathcal{D}}$ for the MPHP $\boldsymbol{q}(t,0)$, $\boldsymbol{p}(t,0)$. They can be computed by expanding $C_{1,2}^{\mathcal{F}},C_{1,2}^{\mathcal{D}}$ in μ. At $\mu=0$, the ''deterministic'' coefficients $C_{1,2}^{\mathcal{D}}$ equal zero; in physical terms, the MPHP is purely fluctuational.

The terms in Eq. (23) proportional to the deterministic coefficients $C_{1,2}^{\mathcal{D}}$ are responsible for the tendency of the extreme paths to diverge from the fixed point $\boldsymbol{q}=\boldsymbol{0}$, which is why in the limit $\mu\to0$ (in which the extreme paths reduce to the MPHP), these coefficients tend to zero. On the other hand, the coefficients $C_{1,2}^{\mathcal{F}}$ take on nonzero values at $\mu=0$. These values can be determined by integrating Eqs. (10), starting from the vicinity of the limit cycle. Therefore, with

account taken of Eqs. (23) and (24), the extreme trajectories in the tube surrounding the MPHP close to the unstable fixed point must be given to leading order in μ by expressions of the form

$$\boldsymbol{q}(t,\mu)=\boldsymbol{X}(t)+\mu\boldsymbol{Y}(t), \quad \boldsymbol{p}(t,\mu)=\hat{\boldsymbol{A}}\boldsymbol{X}(t), \tag{28}$$

$$\boldsymbol{X}(t)\equiv\boldsymbol{q}^{\mathcal{F}}(t), \quad \boldsymbol{Y}(t)\equiv\boldsymbol{q}^{\mathcal{D}}(t).$$

Here the $\mu=0$ trajectory $(\boldsymbol{X}(t),\hat{\boldsymbol{A}}\boldsymbol{X}(t))$ is the incoming MPHP, in the linear approximation. It is a fluctuational trajectory of the type (22), whereas the term $\mu\boldsymbol{Y}(t)$ allows for admixture of some specific deterministic solution $\boldsymbol{Y}(t)$ of the type (21). In Eq. (28) we have neglected a linear term $\propto\mu\boldsymbol{q}^{\mathcal{F}}(t)$ in $\boldsymbol{q}(t)$ and retained only the linear term $\mu\boldsymbol{q}^{\mathcal{D}}(t)$. The term $\mu\boldsymbol{q}^{\mathcal{F}}(t)$ decays in time whereas $\mu\boldsymbol{q}^{\mathcal{D}}(t)$ increases exponentially with t. Therefore, even if $\mu\boldsymbol{q}^{\mathcal{F}}(t_0)$ and $\mu\boldsymbol{q}^{\mathcal{D}}(t_0)$ were of the same order of magnitude at some instant t_0, the term $\mu\boldsymbol{q}^{\mathcal{F}}(t)$ would be exponentially smaller than $\mu\boldsymbol{q}^{\mathcal{D}}(t)$ when $\exp[(\lambda_1+\lambda_2)(t-t_0)]\gg 1$. This is our justification for neglecting the term proportional to $\mu\boldsymbol{q}^{\mathcal{F}}(t)$.

Even if the ''deterministic'' term $\mu\boldsymbol{q}^{\mathcal{D}}(t)$ is small compared to the ''fluctuational'' term $\boldsymbol{X}(t)$ at some instant $t=t_0$, it will eventually become larger than it. Indeed, all extreme trajectories with $\mu\neq 0$ deviate increasingly from the MPHP; in physical terms, they are repelled by the unstable fixed point. However, as seen from Eqs. (21) and (23), their momenta $\boldsymbol{p}(t,\mu)$, unlike their positions $\boldsymbol{q}(t,\mu)$, do not contain exponentially growing terms proportional to $C_{1,2}^{\mathcal{D}}$. In fact, the momentum of any extreme trajectory with $\mu\neq 0$ tends to zero exponentially as $t\to\infty$. Recall that $\boldsymbol{p}=\boldsymbol{0}$ corresponds to deterministic motion, i.e., to $\dot{\boldsymbol{q}}=\boldsymbol{K}(\boldsymbol{q})$. So we deduce that extreme trajectories with $\mu\neq 0$, once they are repelled by the unstable focus, become increasingly deterministic.

We should comment on the extent to which the parametrized extreme trajectories $\boldsymbol{q}(t,\mu)$, $\boldsymbol{p}(t,\mu)$ of Eq. (28) are locally determined, i.e., can be computed from the linearized Hamiltonian (19). The ratio of coefficients $C_1^{\mathcal{F}}$, $C_2^{\mathcal{F}}$ in the expression for the MPHP $\boldsymbol{X}(t)$, which determines the path taken by the MPHP on the stable manifold of the state $\boldsymbol{q}=\boldsymbol{p}=\boldsymbol{0}$ as it approaches the unstable fixed point ($\boldsymbol{q}=\boldsymbol{0}$), is determined by the flow field of extreme trajectories far from the unstable fixed point. I.e., it is ''global.'' On the other hand the shape of the manifold near $\boldsymbol{q}=\boldsymbol{p}=\boldsymbol{0}$ is ''local'': it is determined by the coefficients of the linearized Hamiltonian (19). And the perturbing term $\boldsymbol{Y}(t)$ in Eq. (28), it turns out, is uniquely determined by the constraint equations (26) and (27).

Surprisingly, the linearized equations of motion allow one to determine the singularities of the pattern of extreme paths near the unstable fixed point. The simplest possible singularity is a caustic. A caustic is an envelope of the set of paths of the form (28) on the (q_1,q_2) plane, as shown in Fig. 1. For a one-parameter set of trajectories $\boldsymbol{q}(t,\mu)$, the Jacobian of the transformation from the variables (q_1,q_2) to (t,μ) is equal to zero on the caustic [34,35]. This condition can be written in the form

$$\frac{\partial\boldsymbol{q}(t,\mu)}{\partial t}\wedge\frac{\partial\boldsymbol{q}(t,\mu)}{\partial\mu}=0, \quad \boldsymbol{A}\wedge\boldsymbol{B}\equiv A_1B_2-A_2B_1. \tag{29}$$

Using this condition as well as Eq. (28), one can find a relation between the values of μ and t on the caustic, and an equation for the caustic in parametric form

$$\mu=\mu_c(t)\equiv-\frac{\dot{\boldsymbol{X}}(t)\wedge\boldsymbol{Y}(t)}{\dot{\boldsymbol{Y}}(t)\wedge\boldsymbol{Y}(t)}, \tag{30}$$

$$\boldsymbol{q}_c(t)\equiv\boldsymbol{q}[t,\mu_c(t)]=\boldsymbol{X}(t)+\mu_c(t)\boldsymbol{Y}(t). \tag{31}$$

It will be shown below, using the explicit forms for the fluctuational component $\boldsymbol{X}(t)$ and the deterministic component $\boldsymbol{Y}(t)$, that $\mu_c(t)$ is never equal to zero. This is in agreement with our basic assumption that MPHP never touches a caustic.

The pattern of extreme paths in the vicinity of the unstable fixed point may display a higher-order singularity: a cusp. As shown in Fig. 1, a cusp is a point at which two branches of a caustic merge together, or, in a different phrasing, the caustic stops, and starts moving in the opposite direction. In the parametrization of Eqs. (30) and (31), a point on a caustic is a cusp if and only if

$$\frac{d\boldsymbol{q}_c}{dt}=\boldsymbol{0}. \tag{32}$$

Equation (31) implies that the derivative $d\boldsymbol{q}_c/dt$ is a sum of two vectors, one of which, $\partial\boldsymbol{q}(t,\mu_c(t))/\partial t$, corresponds to the velocity along the extreme trajectory that touches the caustic at the instant t, with the other, $\dot{\mu}_c(t)\boldsymbol{Y}(t)$, arising from the motion of the point of tangency along the caustic due to the dependence of μ_c on t. But it follows from Eq. (29), the condition for a caustic, that these vectors are parallel to each other. Therefore they are also parallel to $\dot{\boldsymbol{q}}_c(t)$, and condition (32) can be reduced to a scalar equation,

$$\mathscr{J}(t)=0, \quad \mathscr{J}(t)\equiv\dot{\boldsymbol{q}}_c(t)\cdot\boldsymbol{Y}(t). \tag{33}$$

A point $\mathbf{q}_c(t)$ on the parametrized caustic is a cusp if and only if t satisfies Eq. (33).

V. A CHANGE OF VARIABLES; CHARACTERISTIC PARAMETERS

The Hamiltonian function H, which is given in the linear approximation near the unstable fixed point by Eq. (19), contains two 2×2 matrices, $\hat{\boldsymbol{d}}$ and $\hat{\boldsymbol{Q}}$, and, hence, seven parameters (the matrix $\hat{\boldsymbol{Q}}$ is symmetric). The actual number of parameters that characterize the flow of extreme paths near the unstable fixed point is smaller. To reveal the relevant parameters we shall make a linear change of variables

$$\boldsymbol{q}'=\hat{\boldsymbol{\Phi}}^{-1}\boldsymbol{q}, \quad \boldsymbol{p}'=\hat{\boldsymbol{\Phi}}^{\dagger}\boldsymbol{p}. \tag{34}$$

The form of the Hamiltonian in the new variables remains the same as in Eq. (19) provided we define new variables

$$\hat{\boldsymbol{d}}'=\hat{\boldsymbol{\Phi}}^{-1}\hat{\boldsymbol{d}}\hat{\boldsymbol{\Phi}}, \quad \hat{\boldsymbol{Q}}'=\hat{\boldsymbol{\Phi}}^{-1}\hat{\boldsymbol{Q}}(\hat{\boldsymbol{\Phi}}^{\dagger})^{-1}. \tag{35}$$

The matrix $\hat{\boldsymbol{A}}$ of Eq. (24), which describes the local shape of the stable manifold of the point $(\boldsymbol{q},\boldsymbol{p})=(\boldsymbol{0},\boldsymbol{0})$, is transformed to

$$\hat{\boldsymbol{A}}' = \hat{\boldsymbol{\Phi}}^{\dagger}\hat{\boldsymbol{A}}\hat{\boldsymbol{\Phi}}. \tag{36}$$

In view of the particular importance of the matrix $\hat{\boldsymbol{A}}$ we shall choose the transformation $\hat{\boldsymbol{\Phi}}$ so that $-\hat{\boldsymbol{A}}'$ is the identity matrix, i.e., $\hat{\boldsymbol{A}}' = -\boldsymbol{I}$.

To find the form of the matrices $\hat{\boldsymbol{d}}', \hat{\boldsymbol{Q}}'$ for which $\hat{\boldsymbol{A}}' = -\boldsymbol{I}$, we first derive an equation that $\hat{\boldsymbol{A}}$ must satisfy. It can be obtained from the zero-energy constraint by substituting Eq. (24) into the quadratic Hamiltonian of Eq. (19), and setting the coefficients of $p_i p_j$ equal to zero. Assuming that the inverse matrix $\hat{\boldsymbol{A}}^{-1}$ exists we obtain the equation

$$\hat{\boldsymbol{d}}\hat{\boldsymbol{A}}^{-1} + \hat{\boldsymbol{A}}^{-1}\hat{\boldsymbol{d}}^{\dagger} + \hat{\boldsymbol{Q}} = \boldsymbol{0}. \tag{37}$$

Equation (37) can be solved using a transformation $\hat{\boldsymbol{U}}$ that diagonalizes the matrix $\hat{\boldsymbol{d}}$, i.e.,

$$(\hat{\boldsymbol{d}}\hat{\boldsymbol{U}})_{ij} = \lambda_j \hat{\boldsymbol{U}}_{ij}\,. \tag{38}$$

The matrix $\hat{\boldsymbol{U}}$ will not necessarily be unitary. One can easily see that

$$[\hat{\boldsymbol{U}}^{-1}\hat{\boldsymbol{A}}^{-1}(\hat{\boldsymbol{U}}^{\dagger})^{-1}]_{ij} = -(\lambda_i + \lambda_j^{*})^{-1}[\hat{\boldsymbol{U}}^{-1}\hat{\boldsymbol{Q}}(\hat{\boldsymbol{U}}^{\dagger})^{-1}]_{ij}\,. \tag{39}$$

Since the diffusion matrix $\hat{\boldsymbol{Q}}$ is symmetric and nonnegative definite, and the eigenvalues λ_i of $\hat{\boldsymbol{d}}$ have positive real parts by assumption, it follows from Eq. (39) that the matrices $-\hat{\boldsymbol{A}}^{-1}$ and $-\hat{\boldsymbol{A}}$ are positive definite (a special, nongeneric case when $\hat{\boldsymbol{Q}}$ is degenerate and is diagonalized by the same transformation as $\hat{\boldsymbol{d}}$ will not be considered in the present paper). These results could equally well be obtained from the expression for $\hat{\boldsymbol{A}}$ in the operator form obtained by Ludwig [18]; see also [42].

A Hermitian matrix $\hat{\boldsymbol{A}}$ can be diagonalized by a transformation of the form (36), containing a unitary matrix $\hat{\boldsymbol{\Phi}}$. If the matrix $\hat{\boldsymbol{\Phi}}$ is nonunitary (i.e., it expands or compresses the coordinate axes), both eigenvalues of $\hat{\boldsymbol{A}}'$ can be made equal to -1. Further unitary transformation will not change $\hat{\boldsymbol{A}}'$, and it is convenient to choose them in such a way that the matrix $\hat{\boldsymbol{Q}}'$ of Eq. (35) be diagonalized, i.e., $Q'_{ij} \propto \delta_{ij}$. It follows from Eq. (37) that if this is done, the matrices $\hat{\boldsymbol{Q}}'$, $\hat{\boldsymbol{d}}'$ will be in the form

$$\hat{\boldsymbol{Q}}' = 2\begin{pmatrix} \eta - a & 0 \\ 0 & \eta + a \end{pmatrix}, \quad \hat{\boldsymbol{d}}' = \begin{pmatrix} \eta - a & b \\ -b & \eta + a \end{pmatrix}. \tag{40}$$

The relationship between the parameters η, a, and b and the eigenvalues λ_1, λ_2 of the matrix of drift coefficients $\hat{\boldsymbol{d}}$ is

$$\eta = \tfrac{1}{2}\mathrm{tr}\hat{\boldsymbol{d}} = \tfrac{1}{2}(\lambda_1 + \lambda_2) > 0, \tag{41}$$

$$\eta^2 - a^2 = \tfrac{1}{4}\det(\hat{\boldsymbol{A}}\hat{\boldsymbol{Q}}) \geqslant 0.$$

Moreover, we have

$$\eta^2 - a^2 + b^2 = \det\hat{\boldsymbol{d}} = \lambda_1\lambda_2 > 0.$$

Since the matrix $\hat{\boldsymbol{Q}}$ is Hermitian, a is real. We may also assume that b is real, which corresponds to the transformation matrix $\hat{\boldsymbol{\Phi}}$ being a real matrix. The signs of a and b are not uniquely determined. The sign of a can be changed by performing the rotation $q'_1 \mapsto q'_2$, $q'_2 \mapsto -q'_1$, whereas the sign of b can be changed by performing a reflection. We adopt the convention

$$\mathrm{sgn}a = \mathrm{sgn}b \tag{42}$$

in what follows.

The parameters η, a, and b fully characterize the fluctuational dynamics of the system near the unstable fixed point. The reason why the local fluctuational dynamics are characterized by only three parameters is that the 2×2 matrices $\hat{\boldsymbol{d}}$ and $\hat{\boldsymbol{Q}}$ together have four invariants, but one of them (i.e., $\mathrm{tr}\hat{\boldsymbol{Q}}$) is irrelevant since it may be absorbed in a multiplicative renormalization of the noise intensity D.

In what follows we assume that the change of variables (34) has been performed, and remove the primes

$$\boldsymbol{q}' \Rightarrow \boldsymbol{q}, \quad \boldsymbol{p}' \Rightarrow \boldsymbol{p}, \quad \hat{\boldsymbol{A}}' \Rightarrow \hat{\boldsymbol{A}}, \quad \hat{\boldsymbol{d}}' \Rightarrow \hat{\boldsymbol{d}}, \quad \hat{\boldsymbol{Q}}' \Rightarrow \hat{\boldsymbol{Q}}. \tag{43}$$

In terms of the new (transformed) variables, the linearized dynamics of the extreme trajectories becomes easy to analyze. It follows from Eqs. (24) and (40) that the fluctuational trajectories of the form (23) must satisfy

$$\boldsymbol{p}^{\mathcal{F}}(t) = -\boldsymbol{q}^{\mathcal{F}}(t). \tag{44}$$

Moreover, Hamilton's equations of motion, which the MPHP $\boldsymbol{X}(t)$ and the admixed deterministic trajectory $\boldsymbol{Y}(t)$ must satisfy, in terms of the new variables simplify to yield

$$\frac{d\boldsymbol{X}}{dt} = -\hat{\boldsymbol{d}}^{\dagger}\boldsymbol{X}, \quad \frac{d\boldsymbol{Y}}{dt} = \hat{\boldsymbol{d}}\boldsymbol{Y}, \tag{45}$$

$$\boldsymbol{p}(t) = -\boldsymbol{X}(t).$$

That is, in terms of the new variables the equations of motion for $\boldsymbol{X}(t)$ and $\boldsymbol{Y}(t)$ *separate*. The constraint (27) on the vectors $\boldsymbol{X}, \boldsymbol{Y}$ takes the form

$$\dot{\boldsymbol{Y}}\cdot\boldsymbol{X} = \boldsymbol{Y}\cdot\dot{\boldsymbol{X}} = \boldsymbol{0}. \tag{46}$$

This means that the basis in which the matrix $\hat{\boldsymbol{A}}$ equals $-\hat{\boldsymbol{I}}$ has a simple physical interpretation. In this basis one of the axes ($\dot{\boldsymbol{X}}$) is locally tangent to the MPHP and the other axis ($\boldsymbol{Y}$) is perpendicular to the MPHP.

If we parametrize the extreme trajectories in the vicinity of the unstable fixed point by t and μ as in Eq. (28), with t measured from an instant t_0 which we choose to be equal to zero, the zero-energy classical action S as a function of position will be a function of t and μ

$$S = \int \boldsymbol{p}\cdot\dot{\boldsymbol{q}}dt = S(t,\mu). \tag{47}$$

With account taken of Eqs. (27), (28), (45) we have

$$S(t,\mu)=S(0,\mu)+\int_0^t \boldsymbol{p}\cdot\dot{\boldsymbol{q}}dt=S(0,\mu)-\frac{1}{2}\boldsymbol{X}^2(t). \quad (48)$$

We shall compute the action relative to its value at the unstable fixed point, i.e., relative to $S_f\equiv S(t=\infty,\mu=0)$. Since $\partial S/\partial \boldsymbol{q}=\boldsymbol{p}$ and $\boldsymbol{q}(0,\mu)-\boldsymbol{q}(0,0)\approx\mu\boldsymbol{Y}(0)$ [see Eq. (28)], Eqs. (45), (48) imply

$$s(0,\mu)=-\mu\boldsymbol{X}(0)\cdot\boldsymbol{Y}(0), \quad (49)$$

and

$$s(t,\mu)=-\tfrac{1}{2}\boldsymbol{X}^2(t)-\mu\boldsymbol{X}(0)\cdot\boldsymbol{Y}(0), \quad (50)$$

where

$$s(t,\mu)\equiv S(t,\mu)-S_f \quad (51)$$

is the normalized action. Equation (50) provides a simple explicit expression, valid in the vicinity of the unstable fixed point, for the action as a function of time, and of the variable μ that indexes the extreme trajectories.

The function $S(t,\mu)$ is of course single valued. However, the action as a function of *position* $\boldsymbol{q}$ is multiple valued, since extreme trajectories $\boldsymbol{q}(t,\mu)$ with different (t,μ) may cross each other. The optimal path to a given point $\boldsymbol{q}$, as we have explained, is the extreme path with minimum action. It is worth noting that this must be no greater than S_f. Indeed, from the unstable fixed point $\boldsymbol{q}=\boldsymbol{0}$ the system can reach any point $\boldsymbol{q}$ without ''building up'' any additional action, merely by moving along a deterministic trajectory $\boldsymbol{q}^{\mathcal{D}}(t)$ of the form given by Eq. (21).

VI. OPTIMAL PATHS IN THE ABSENCE OF CUSP POINTS

We can apply the linearized theory of Secs. IV and V to the case when the unstable fixed point, near which the linearization is performed, is a focus. In this case the eigenvalues λ_1, λ_2 of the linearized drift matrix $\hat{\boldsymbol{d}}$ are complex with the same (positive) real part, and according to Eq. (40),

$$\lambda_{1,2}=\eta\pm i\omega, \quad \omega^2=b^2-a^2. \quad (52)$$

With account taken of the orthogonality condition (46) that the two fundamental trajectories $\boldsymbol{X}(t)$ and $\boldsymbol{Y}(t)$ must satisfy, we may solve Hamilton's equations (45) to obtain

$$\boldsymbol{X}(t)=\kappa\exp(-\eta t)\boldsymbol{R}(\theta,\gamma), \quad (53)$$

$$\boldsymbol{Y}(t)=\exp(\eta t)\boldsymbol{R}(\theta+\phi,\gamma^{-1}), \quad (54)$$

where

$$\boldsymbol{R}(\theta,\gamma)\equiv\boldsymbol{e}_1\cos\theta-\gamma\boldsymbol{e}_2\sin\theta.$$

Here $\theta=\omega t$, and

$$\phi=\arctan\left(\frac{\eta}{\omega}\right), \quad \gamma=\left(\frac{b+a}{b-a}\right)^{1/2}\mathrm{sgn}b, \quad \boldsymbol{e}_{1,2}=\begin{pmatrix}\pm\frac{1}{\sqrt{2}}\\ \frac{1}{\sqrt{2}}\end{pmatrix}. \quad (55)$$

The two functions $\boldsymbol{X}(t)$ and $\boldsymbol{Y}(t)$, when graphed, yield *spirals*: they wind in (i.e., toward the unstable focus) and out (i.e., away from the unstable focus), respectively. The converging spiral $\boldsymbol{X}(t)$, which is incident on the unstable focus as $t\to\infty$, is the MPHP. The two spirals have the same angular frequency ω, and pitches $\pm\eta$ that are of equal magnitude and opposite sign. They have the same direction of rotation about the focus; the direction is determined by $\mathrm{sgn}b$. The *shape* of the two spirals is determined by the periodic vector-function $\boldsymbol{R}(\theta,\gamma)=\boldsymbol{R}(\theta+2\pi,\gamma)$. This function is a parametric representation of an ellipse whose principal axes are directed along the unit vectors $\boldsymbol{e}_{1,2}$. As a consequence, the spirals are elliptic rather than circular. The ratio between the length of the major axis and the minor axis of the ellipse is $|\gamma|$ [according to Eqs. (42) and (54], $|\gamma|>1$). The quantity ϕ can be viewed as a phase difference between the two spirals.

The quantity κ in the equation for $\boldsymbol{X}(t)$ is a *globally determined parameter*. It cannot be computed in the framework of the linearized model (18)–(20), and it distinguishes the MPHP from the other ''fluctuational'' solutions of the form (22) that are incident on the focus and may also be described by Eq. (53), with κ ranging over the interval

$$\kappa_1\exp(-2\pi\eta/\omega)\leqslant\kappa<\kappa_1,$$

with κ_1 arbitrary.

Extreme paths other than the MPHP also spiral down toward the unstable focus, but only initially. We may write them in the ''normal form'' (28) with $\mu\neq0$, i.e., as $\boldsymbol{q}(t,\mu)=\boldsymbol{X}(t)+\mu\boldsymbol{Y}(t)$. Such perturbations of the MPHP (which has $\mu=0$) will remain close to the MPHP on a time scale $t\lesssim1/(2\eta)\ln\mu^{-1}$. However, we saw in Sec. IV B that extreme paths other than the MPHP eventually become ''deterministic'' rather than fluctuational. The contribution of the unwinding spiral $\mu\boldsymbol{Y}(t)$ increases as t increases, and when the extreme path reaches a distance $\sim|\mu\kappa|^{1/2}$ from the focus the contribution of the unwinding spiral becomes of the same order of magnitude as the contribution of the inward spiraling MPHP, $\mu\boldsymbol{X}(t)$. At that point the extreme path will begin to spiral back out. At times $t\gg\eta^{-1}\ln(\kappa|\mu|)$ the term $\mu\boldsymbol{Y}(t)$ dominates, the motion of the extreme path becomes largely ''deterministic'' and the action $s(t,\mu)$ along the path approaches its asymptotic value $-\mu\boldsymbol{X}(0)\boldsymbol{Y}(0)=-\kappa\mu\cos\phi$. In the $t\to\infty$ limit, the extreme path will spiral back into the stable limit cycle, from which it emerged.

A. The caustic spiraling down to the unstable focus

The location of the caustic occurring in the flow field of extreme paths can be found by substituting Eqs. (53) and (54) into Eqs. (30) and (31). The value of the parameter μ on the caustic turns out to be

$$\mu_c(t) = -\kappa \exp(-2\eta t)\frac{1+\gamma^2}{2\cos\phi}\left(1+\frac{\gamma^2-1}{\gamma^2+1}\cos 2(\omega t+\phi)\right). \tag{56}$$

The caustic itself may be written in a parametric form [cf. Eq. (31)] as

$$\boldsymbol{q}_c(t) = \boldsymbol{X}(t) + \mu_c(t)\boldsymbol{Y}(t) = \kappa \exp(-\eta t)\boldsymbol{z}(\omega t), \tag{57}$$

where $\boldsymbol{z}(\theta)$ is a ''locally determined'' (rather than globally determined, in the sense mentioned above) function that has period 2π. Equation (57) is the equation of a curve that spirals down to the focus. It follows from Eq. (56) that μ_c is always nonzero, which is an important point: it proves self-consistency of our assumption that the MPHP (the extreme path with zero μ) never encounters a caustic. We notice that irrespective of the detailed form of the caustic, the function $q_c(t)$ is self-similar: the amplitude [$\propto \kappa \exp(-\eta t)$] changes from one turn to the next, but the shape of each successive turn is the same. *The caustic is self-similar.*

In the remainder of Sec. VI we shall investigate the case when there are no cusp points on the caustic in the vicinity of the fixed point $\boldsymbol{q}=\boldsymbol{0}$ where the linear approximation (19) applies. This means that $\dot{\boldsymbol{q}}_c(t)$ does not become equal to zero, i.e., the quantity $\mathcal{L}(t) \equiv \boldsymbol{Y}(t)\cdot\dot{\boldsymbol{q}}_c(t)$ is never zero [see Eq. (33)]. Using the explicit expressions (54), (56) one can show that

$$\begin{aligned}\mathcal{L}(t) \equiv \boldsymbol{Y}(t)\cdot\dot{\boldsymbol{q}}_c(t) = {} & \frac{\kappa}{4\gamma^2\cos\phi}[4\gamma^2+1+(\gamma^2-1)\cos 2\theta] \\ & \times\{\eta(\gamma^2+1)+(\gamma^2-1)[\eta\cos 2(\theta+\phi) \\ & +3\omega\sin 2(\theta+\phi)]\}. \end{aligned} \tag{58}$$

The condition for $\dot{\boldsymbol{q}}_c(t)$ not to become equal to zero is therefore of the form

$$\frac{\gamma^2-1}{\gamma^2+1}\frac{\sqrt{\eta^2+9\omega^2}}{\eta} < 1, \text{ or } \eta > 3|a|, \tag{59}$$

when expressed in terms of the characteristic parameters of the model. An expression for the action on the caustic, $s_c = s_c(t)$, can be obtained from the equation

$$\frac{ds_c}{dt} = \nabla s(\boldsymbol{q}_c(t))\dot{\boldsymbol{q}}_c(t) = -\boldsymbol{X}(t)\dot{\boldsymbol{q}}_c(t), \quad s_c(t) \equiv s_c(\boldsymbol{q}_c(t)). \tag{60}$$

Clearly, the sign of $\dot{s}_c$ changes at the cusp points on the caustic, if any ($\dot{\boldsymbol{q}}_c=\boldsymbol{0}$). Using Eqs. (53) and (54), and (56) one can show that if the condition (59) is satisfied, the derivative $\dot{s}_c$ is always negative. In this case the action on the caustic

$$\begin{aligned} s_c(t) = {} & \frac{\kappa^2}{4}\exp(-2\eta t)\{1+\gamma^2+(\gamma^2-1) \\ & \times[\cos 2\omega t + 2\cos 2(\omega t+\phi)]\}, \end{aligned} \tag{61}$$

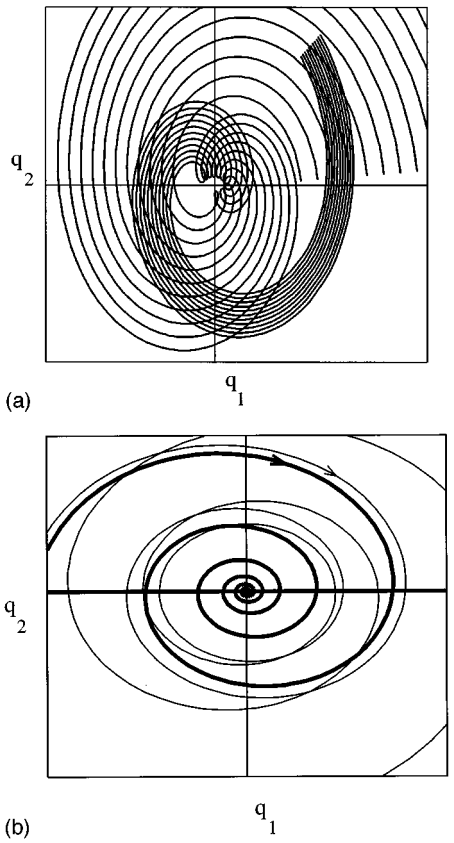

FIG. 2. Extreme paths near the unstable focus at $\boldsymbol{q}=\boldsymbol{0}$. The parameters specifying local dynamics [see Eqs. (41) and (52)] are $a=0.13$, $\omega=3.5$, and $\eta=0.41$. The axes are scaled by the parameter κ of Eq. (53). (a) Paths with $\mu/\kappa<0$; such paths are reflected from a caustic that spirals down to the focus. (b) The MPHP (most probable hitting path), which spirals down to the focus (in bold), and a path with $\mu/\kappa>0$, which initially spirals in, but eventually spirals out without encountering the caustic.

decreases monotonically with increasing t. In other words, the action on the caustic always exceeds its value at the unstable fixed point $\boldsymbol{q}=\boldsymbol{0}$, and it increases monotonically away from this point.

By construction the caustic is tangent to extreme paths $\boldsymbol{q}(t)=\boldsymbol{X}(t)+\mu\boldsymbol{Y}(t)$ with nonzero μ. The caustic is encountered by an extreme path $\boldsymbol{X}(t)+\mu\boldsymbol{Y}(t)$ if and only if the equality $\mu=\mu_c(t)$ is satisfied. At the tangency point the velocity on the path $\dot{\boldsymbol{q}}(t)=\dot{\boldsymbol{X}}(t)+\mu_c(t)\dot{\boldsymbol{Y}}(t)$ may be parallel or antiparallel to the velocity of the caustic $\boldsymbol{q}_c(t)$. It turns out that the vector $\dot{\boldsymbol{q}}(t)$ is antiparallel to $\dot{\boldsymbol{q}}_c(t)$ at the tangency point, i.e., $\dot{\boldsymbol{q}}(t)\cdot\dot{\boldsymbol{q}}_c(t)<0$. This can be seen by comparing the signs of $\boldsymbol{Y}(t)\cdot\dot{\boldsymbol{q}}_c(t)$ and $\boldsymbol{Y}(t)\cdot\dot{\boldsymbol{q}}(t)$; we omit the computation.

In models with $\kappa>0$, $\gamma>1$, the function $\mu_c(t)$ of Eq. (56) takes on only negative values. As a result, extreme trajectories with $\mu<0$ encounter (and are reflected from) the caustic, whereas extreme trajectories with $\mu>0$ do not touch the caustic. In Fig. 2(a) we show an initially narrow tube of extreme trajectories that emanate from the limit cycle, and spiral toward the unstable focus, but then encounter the caustic, and spiral away from the focus.

In the absence of cusp points on the caustic (a possibility that we consider in Sec. VII), the vector $\boldsymbol{q}_c(t)$ will rotate in

the same direction as $\boldsymbol{Y}(t)$ and $\boldsymbol{X}(t)$, and as t increases, the direction of this rotation will not reverse. Most of the time, extreme trajectories $\boldsymbol{X}(t)+\mu\boldsymbol{Y}(t)$ that are perturbations of the MPHP rotate in this direction as well. However, in the region of the system state space where the extreme trajectories encounter the caustic, they make a loop, so that their velocity is opposite to that of the caustic.

B. The self-similar topology of the Lagrangian manifold

In the linear approximation near the unstable focus, the Lagrangian manifold $\boldsymbol{p}=\boldsymbol{p}(\boldsymbol{q})$ is traced out by the extreme trajectories $\boldsymbol{X}(t)+\mu\boldsymbol{Y}(t)$ with different values of the mixing parameter μ. It is given in parametric form, with parameters (t,μ), by

$$\boldsymbol{q}(t,\mu)=\boldsymbol{X}(t)+\mu\boldsymbol{Y}(t), \tag{62}$$

$$\boldsymbol{p}(t,\mu)=-\boldsymbol{X}(t). \tag{63}$$

Here the inward and outward spirals, $\boldsymbol{X}(t)$ and $\boldsymbol{Y}(t)$, are defined in Eqs. (53) and (54). It follows from Eqs. (62) and (63) that the LM is invariant with respect to a transformation which includes a rotation of coordinates by π radians, and a simultaneous rescaling of variables. In polar coordinates (q,Θ) defined by

$$q_1=q\cos\Theta, \quad q_2=q\sin\Theta, \tag{64}$$

such a transformation would alter the angular coordinate Θ according to

$$\Theta\mapsto\Theta\mp\pi\ \mathrm{sgn}b. \tag{65}$$

In terms of the phase space coordinates $\boldsymbol{q}$ and $\boldsymbol{p}$, the transformation would take the form

$$\boldsymbol{q}\mapsto-\exp\left(\mp\frac{\pi\eta}{\omega}\right)\boldsymbol{q}, \tag{66a}$$

$$\boldsymbol{p}\mapsto-\exp\left(\mp\frac{\pi\eta}{\omega}\right)\boldsymbol{p}. \tag{66b}$$

The transformation law (66) can be understood from the fact that at a given instant of time all points $\boldsymbol{q}(t,\mu)\equiv\boldsymbol{X}(t)+\mu\boldsymbol{Y}(t)$ on the (q_1,q_2) plane, regardless of the value of μ, have their momenta equal to $-\boldsymbol{X}(t)$. Over half the period π/ω, the vector $\boldsymbol{X}(t)+\mu\boldsymbol{Y}(t)$ rotates around the point $\boldsymbol{q}=\boldsymbol{0}$ by an angle $-\pi\,\mathrm{sgn}b$. As a result of the rotation, each point $\boldsymbol{q}(t,\mu)$ goes over into $\boldsymbol{q}(t+\pi/\omega,\mu\exp(-2\pi\eta/\omega))$. The only Hamiltonian trajectory that remains invariant under the transformation (66) is the MPHP (for which $\mu=0$).

All extreme trajectories lie on the zero-energy surface in phase space, i.e., satisfy the zero-energy constraint $H(q_1,q_2,p_1,p_2)=0$. But the Hamiltonian function H of Eq. (19) is quadratic in p_1 and p_2. Therefore, at each specified q_1,q_2,p_1, the momentum component p_2 takes one of two possible values compatible with the condition $H=0$. The shape of the Lagrangian manifold $\boldsymbol{p}=\boldsymbol{p}(q_1,q_2)$ can be understood from an analysis of the surface $p_1=p_1(q_1,q_2)$. Portions of this surface are shown in Fig. 3(a). The values of

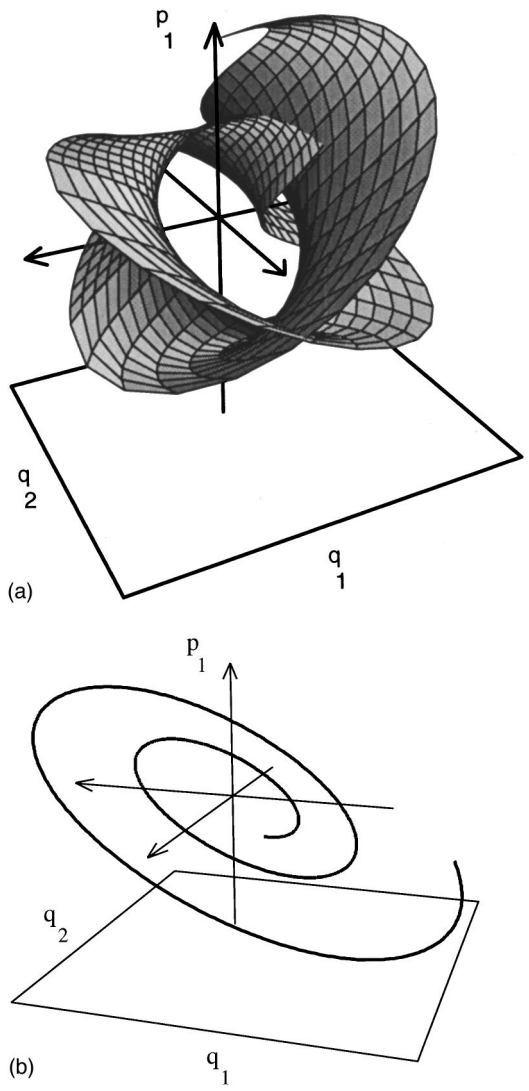

FIG. 3. (a) A turn (two branches on opposite sides of a fold) of the surface $p_1=p_1(\boldsymbol{q})$ near the unstable fixed point $\boldsymbol{q}=\boldsymbol{0}$. Parameter values are $a=0.03$, $\omega=3.9$, and $\eta=0.41$. (b) The position of the fold in the surface $p_1=p_1(\boldsymbol{q})$.

$p_2(p_1,q_1,q_2)$ on the intersecting sheets of $p_1(\boldsymbol{q})$ are different: in general, the LM is not self-intersecting in the four-dimensional phase space whose coordinates are q_1,q_2,p_1,p_2. One can think of the surface $p_1=p_1(\boldsymbol{q})$ as an infinitely long sheet that is first folded, and then twisted in such a way that the fold is wound into a curve that spirals down to the point $\boldsymbol{q}=\boldsymbol{p}=\boldsymbol{0}$. This spiral is shown in Fig. 3(b).

The projection of the fold on the $\boldsymbol{q}$ plane is the caustic, and the equation for the spiral in Fig. 3(b), in parametric form, is $\boldsymbol{q}=\boldsymbol{X}(t)+\mu_c(t)\ \boldsymbol{Y}(t)$, $\boldsymbol{p}=-\boldsymbol{X}(t)$. We note that self-intersections of the surface $p_1=p_1(\boldsymbol{q})$ arise not only from the nonmonotonic dependence of the ''height'' of the fold p_1 on the radius $q\equiv|\boldsymbol{q}|$; there are also self-intersections of the sides of the sheet $p_1(\boldsymbol{q})$ on opposite sides of the fold, which make Fig. 3(a) look as complicated as it does. Alternatively, the surface $p_1=p_1(\boldsymbol{q})$ may be compared to a whorl that spirals down to the point $\boldsymbol{q}=\boldsymbol{0}$, $p_1=0$. The whorl is unusual; its turns go up and down, and the step size steadily decreases with the number of turns.

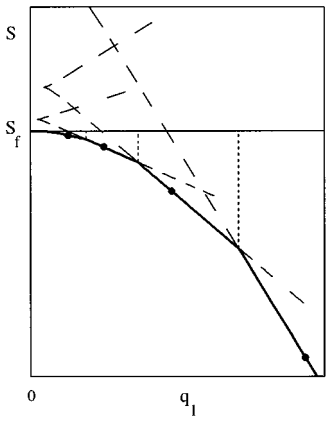

FIG. 4. Cross sections of two turns of the surface $p_1=p_1(\boldsymbol{q})$ of Fig. 3(a). Here $q_2=0$. The turn II is the turn I after one revolution over the p_1 axis, i.e., with Θ of Eq. (66) increased by 2π. Parameters are the same as in Fig. 3. The successive intersections of the MPHP with the $q_2=0$ plane are shown with filled circles. Over the revolution, the extreme trajectory 1 passes through the fold (its projection is reflected by the caustic), and goes from the lower to the upper sheet of $p_1(\boldsymbol{q})$. Trajectory 2 always stays on the side opposite to the caustic with respect to the MPHP. The solid line that starts at the origin and passes through the filled circles is the cross section of the stable manifold of the fixed point to which MPHP belongs.

Additional insight into the structure of the surface $p_1=p_1(\boldsymbol{q})$ can be gained from a Poincaré section by a vertical half-plane. (See Fig. 4; for convenience we choose the half-plane to be $q_2=$const, $q_1\geqslant 0$.) Successive branches of the cross section are partly ''nested'' into one another. The pattern of branches is self-similar: any branch can be obtained from any other by (repeatedly) applying transformations of the form (66). We note that outside the small-q range, where a linearized treatment is not valid, the transformation law (66) must be modifed. So the surface $p_1=p_1(\boldsymbol{q})$, like the caustic, is really only *asymptotically* self-similar. Incidentally, the sheets of the surface $\boldsymbol{p}=\boldsymbol{p}(\boldsymbol{q})$, which appear separate at small q, are connected to each other at large q. To study the way in which they are connected, one would have to go beyond the linear approximation.

The surface $p_2(\boldsymbol{q})$ is similar to the surface $p_1(\boldsymbol{q})$, so that the Lagrangian manifold $\boldsymbol{p}=\boldsymbol{p}(\boldsymbol{q})$ is a two-dimensional *helicoidal surface* $\boldsymbol{p}=\boldsymbol{p}(\boldsymbol{q})$ in the four-dimensional phase space. On this surface, the fold $(\boldsymbol{q}_c(t),-\boldsymbol{X}(t))$ spirals down to the unstable fixed point. The behavior of the extreme trajectories $\boldsymbol{q}(t)$ on the $\boldsymbol{q}$ plane can be qualitatively understood from the behavior of the trajectories $(\boldsymbol{q}(t),\boldsymbol{p}(t))$ on one of the surfaces $p_i=p_i(\boldsymbol{q})$ $(i=1$ or $2)$. One such trajectory is $(\boldsymbol{q}^{\mathcal{F}}(t),\boldsymbol{p}^{\mathcal{F}}(t))$; its projection is the MPHP. For this trajectory $\boldsymbol{p}=-\boldsymbol{q}$, i.e., the trajectory corresponds to the intersection of the surface $p_1=p_1(q_1,q_2)$ and the plane $p_1=-q_1$ in the three-dimensional (q_1,q_2,p_1) space. We note that the LM is the unstable manifold of the limit cycle [the periodic orbit $\boldsymbol{q}=\boldsymbol{q}^{(cl)}(t)$, $\boldsymbol{p}=\boldsymbol{0}$], whereas the hyperplane $\boldsymbol{p}=-\boldsymbol{q}$ is the stable manifold of the fixed point $\boldsymbol{q}=\boldsymbol{p}=\boldsymbol{0}$. The trajectory $(\boldsymbol{q}^{\mathcal{F}}(t),\boldsymbol{p}^{\mathcal{F}}(t))$ is the heteroclinic trajectory along which the two manifolds intersect.

The behavior of the remaining Hamiltonian trajectories on the surface $p_1=p_1(\boldsymbol{q})$ is easy to analyze. It follows from Eqs. (28) that trajectories $(\boldsymbol{q}=\boldsymbol{X}(t)+\mu\boldsymbol{Y}(t),p_1(t)=-X_1(t))$ with opposite signs of μ deviate from the heteroclinic trajectory $(\boldsymbol{q}^{\mathcal{F}}(t),p_1^{\mathcal{F}}(t))$ in opposite directions. The Hamiltonian trajectories that go toward the fold of the surface $p_1=p_1(\boldsymbol{q})$ are those with negative μ [their projections $\boldsymbol{X}(t)+\mu\boldsymbol{Y}(t)$ go toward the caustic]. They spiral around the point $\boldsymbol{q}=\boldsymbol{0}$ and approach it, then they go over the fold (at which time their projections are reflected from the caustic) and spiral away from the axis $\boldsymbol{q}=\boldsymbol{0}$. [The behavior of their projections is shown in Fig. 2(a)]. None of the trajectories passes through the fold more than once. Indeed, the fold is only passed when $\mu=\mu_c(t)$, where $\mu_c(t)$ is given by Eq. (56). In the range (59), the function $\mu_c(t)$ is a monotonic function of t, so the equation $\mu=\mu_c(t)$ cannot have more than a single solution.

The Hamiltonian trajectories $\boldsymbol{q}(t)=\boldsymbol{X}(t)+\mu\boldsymbol{Y}(t)$, $p_1(t)=-X_1(t)$ with positive μ deviate from the heteroclinic trajectory $(\boldsymbol{q}^{\mathcal{F}}(t),p_1^{\mathcal{F}}(t))$ in the direction opposite to the fold, therefore they never cross over the fold. At comparatively small t they spiral around the axis $\boldsymbol{q}=\boldsymbol{0}$ and approach it, as does $(\boldsymbol{q}^{\mathcal{F}}(t),p_1^{\mathcal{F}}(t))$, but then, as the amplitude of the outward-spiraling component $\mu\boldsymbol{Y}(t)$ increases, they begin to spiral away from $\boldsymbol{q}=\boldsymbol{0}$. The behavior of the projections $\boldsymbol{q}=\boldsymbol{q}(t)$ of these trajectories is shown in Fig. 2(b).

Successive positions of points on trajectories with $\mu=0$, $\mu<0$, and $\mu>0$, on the Poincaré section of the surface $p_1=p_1(\boldsymbol{q})$, are shown in Fig. 4 (by filled circles, and empty circles; 1, 1′ and 2, 2′, respectively).

In the limit of large t the Hamiltonian trajectories with $\mu>0$ and $\mu<0$ display similar asymptotic behavior. In this limit the momentum $\boldsymbol{p}(t)=-\boldsymbol{X}(t)$ tends to zero, and the trajectories approach deterministic trajectories of the form $\boldsymbol{q}(t)\propto\boldsymbol{Y}(t)$, $\boldsymbol{p}=\boldsymbol{0}$, which wind away from the point $\boldsymbol{q}=\boldsymbol{0}$. The sheets of $p_1=p_1(\boldsymbol{q})$ accordingly *accumulate* near the plane $p_1=0$.

The topology of the surface $p_1=p_1(\boldsymbol{q})$ explains why infinitely many extreme paths $\boldsymbol{q}(t)$ pass through any point $\boldsymbol{q}'$ in the vicinity of $\boldsymbol{q}=\boldsymbol{0}$, as shown in Figs. 2(a), 2(b). Different paths $\boldsymbol{q}(t)$ lie on different sheets of $p_1=p_1(\boldsymbol{q})$, and some of the paths (those with $\mu<0$) start spiraling away from the point $\boldsymbol{q}=\boldsymbol{0}$ after they encounter the caustic, and are reflected from it (i.e., when the Hamiltonian trajectories pass through the fold), whereas the others (those with $\mu>0$) do so without encountering the caustic. A natural question is, which of the extreme paths that are incident on a given point $\boldsymbol{q}'$ is *physically observable*, i.e., is optimal. To answer this question, we must determine for which of the extreme paths the action is a minimum.

C. The multivalued action and the switching line

The value of the normalized action $s\equiv S-S_f$ is unique for a given extreme path, and therefore s is uniquely defined as a function on the Lagrangian manifold. The Lagrangian manifold, as a two-dimensional surface in the four-dimensional phase space whose coordinates are $(\boldsymbol{q},\boldsymbol{p})$, is defined by the function $\boldsymbol{p}=\boldsymbol{p}(\boldsymbol{q})$. Since this function is multi-

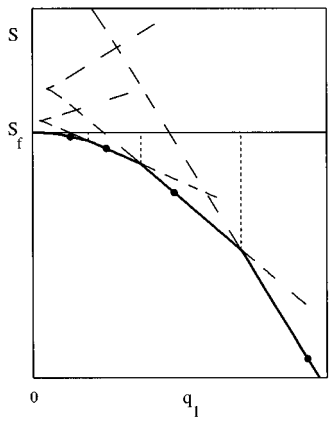

FIG. 5. A cross section of the action surface $S=S(q_1,q_2)$ near the unstable focus $\boldsymbol{q}=\mathbf{0}$. Here $q_2=0$, and S_f is the action at the focus. The surface of minimum action, $S_{\min}=S_{\min}(q_1,q_2)$, is shown in bold. The nonoptimal pieces of the action surface are shown dashed. Parameter values are the same as in Fig. 3. The cusp points of the multivalued function $S=S(q_1,0)$ are cross sections of the spinode edge of $S(q_1,q_2)$, which corresponds to the caustic. These cusp points are located at the values of q_1 at which the slope $dp_1(q_1,0)/dq_1$, as plotted in Fig. 4, becomes infinite.

valued (the manifold may fold over on itself, as we have seen), if s is viewed as a function of $\boldsymbol{q}$, then it too will be multivalued.

A cross section of the surface $s=s(\boldsymbol{q})$, corresponding to the cross section of the surface $p_1=p_1(\boldsymbol{q})$ shown in Fig. 4, is shown in Fig. 5. The multivaluedness is obvious. The same half-plane $q_2=0$, $q_1\geqslant 0$, is used as in Fig. 4, but more branches are displayed. The cusps in the graph of $s=s(\boldsymbol{q})$, as shown in Fig. 5, arise from extrema of the curves $p_1=p_1(q_1)$ of Fig. 4, i.e., from points where $dp_1/dq_1=\infty$. These are points that lie on the caustic. As computed previously, the value of s on the caustic is the positive quantity denoted s_c, which increases monotonically away from the caustic.

The value of $s(q_1)$ on each branch is given by the expression

$$s_n^{(i)}(q_1)=s_c^{(i)}+\int p_n^{(i)}(q_1,q_2=0)dq_1, \tag{67}$$

where the superscript i enumerates the cusp points (i.e., the pairs of branches of p_1), and the subscript $n=1,2$ enumerates the branches that merge at the point where $dp_1/dq_1=\infty$.

It is clear from Fig. 5 that the surface of *minimum* action $s_{\min}=s_{\min}(\boldsymbol{q})$ is only piecewise smooth. The existence of a minimum action at each $\boldsymbol{q}$ follows from the fact that, although the number of extreme paths $t\mapsto\boldsymbol{q}(t)$ passing through any given point $\boldsymbol{q}'$ is infinite, the normalized action function $s(\boldsymbol{q})=S(\boldsymbol{q})-S_f$ is bounded from below by $-S_f$ [since $S(\boldsymbol{q})>0$, see Eq. (12)]. The cross section of the surface $s_{\min}(\boldsymbol{q})$ is shown in bold in Fig. 5. This figure provides an intuitive picture of the structure of the surface of minimum action as consisting of sections that correspond to sections of different sheets of the LM. Quantitative analysis of $s_{\min}(\boldsymbol{q})$ is facilitated by the fact that at any point along the MPHP, minimum action is achieved if the system moves along the MPHP. This fact can be verified as follows. The condition that an extreme path intersect with another extreme path is of the form

$$\boldsymbol{q}(t_1,\mu_1)=\boldsymbol{q}(t_2,\mu_2). \tag{68}$$

Equation (68) has a countable set of solutions for each $\boldsymbol{q}(t_1,\mu_1)$. For a point on the MPHP ($\mu_1=0$) we have

$$\boldsymbol{X}(t_1)=\boldsymbol{X}(t_2)+\mu_2\boldsymbol{Y}(t_2). \tag{69}$$

Using the expression (50) for the action $s(t,\mu)$ and the identity

$$\boldsymbol{X}(t)\cdot\boldsymbol{Y}(t)=\kappa\cos\phi \tag{70}$$

that follows from Eqs. (53), (54), one can easily compute from Eq. (69) that the difference between the actions for the MPHP and an alternative path satisfies

$$s(t_1,0)-s(t_2,\mu_2)=-\mu_2^2\boldsymbol{Y}(t)^2<0. \tag{71}$$

This proves that the MPHP is indeed the optimal path to every point along its extent, including the unstable focus $\boldsymbol{q}=\mathbf{0}$.

It is clear that points $\boldsymbol{q}$ very close to points on the MPHP are reached preferentially along extreme paths very close to the MPHP, i.e., extreme paths with $|\mu\boldsymbol{Y}(t)|\ll|\boldsymbol{X}(t)|$. However, the MPHP is a spiral. When one moves transverse to the spiral one goes from the vicinity of one turn to the vicinity of the next (or former) turn. Clearly, somewhere along the way there should occur a transition between the paths that provide minimum action. The condition for switching is that the actions for the two paths coming to a given point be equal, i.e.,

$$s(t_1,\mu_1)=s(t_2,\mu_2). \tag{72}$$

[We emphasize that it is the *minimum* values of $s(t,\mu)$ for a given $\boldsymbol{q}=\boldsymbol{q}(t,\mu)$ that must coincide.]

Equations (68), (72) can be solved for $\mu_{1,2}$, using Eqs. (50), and (53) and (54). One obtains

$$\mu_i=M(t_i,t_{3-i}),\quad i=1,2, \tag{73}$$

where

$$M(t',t'')\equiv\kappa\exp[-\eta(t'+t'')]\frac{\{\boldsymbol{R}(\omega t'',\gamma)-\exp[-\eta(t'-t'')]\boldsymbol{R}(\omega t',\gamma)\}\wedge\boldsymbol{R}(\omega t''+\phi,\gamma^{-1})}{\boldsymbol{R}(\omega t'+\phi,\gamma^{-1})\wedge\boldsymbol{R}(\omega t''+\phi,\gamma^{-1})}. \tag{74}$$

Substituting the expressions for $\mu_{1,2}$ into Eq. (72), we obtain an algebraic equation that relates t_2 and t_1. Using Eqs. (50) and (70), one can write this equation in the form

$$\tilde{s}(t_1,t_2)=\tilde{s}(t_2,t_1), \tag{75}$$

where

$$\tilde{s}(t',t'')\equiv-\tfrac{1}{2}\kappa^2\exp(-2\eta t')\boldsymbol{R}^2(\omega t',\gamma)-\kappa M(t',t'')\cos\phi.$$

Here $\tilde{s}(t_1,t_2)$ is the minimum value of the action $s(t_1,M(t_1,t_2))$ for a given $\boldsymbol{q}=\boldsymbol{q}(t_1,M(t_1,t_2))$. Equation (75), which is the condition for switching, yields

$$\begin{aligned}\boldsymbol{q}_s(t_1)&=\boldsymbol{q}(t_1,M(t_1,t_2(t_1)))\\&=\boldsymbol{X}(t_1)+M(t_1,t_2(t_1))\boldsymbol{Y}(t_1)\end{aligned} \tag{76}$$

as the parametric equation of the switching line.

We note briefly that at some instant t_1^*, the algebraic equation (75) may have two solutions for the same minimum value of the action. In such a case *three* distinct optimal paths are incident on a single point, rather than two (as in the case of a conventional switching line). We mentioned this possibility briefly in Sec. III A. At such a point two switching lines intersect meet each other and terminate, and a third switching line begins. We shall refer to this phenomenon as a ''branched,'' or ''multibranched'' switching line.

D. Self-similarity of the minimum action surface and the switching line

Both the switching line whose position is given by Eq. (76), and the surface of minimum action $s_{\min}=s_{\min}(\boldsymbol{q})$, are *self-similar*, as is the Lagrangian manifold [see Eqs. (66)]. Self-similarity of $s_{\min}(\boldsymbol{q})$ is a consequence of the self-similarity of the whole surface $s=s(\boldsymbol{q})$. The latter follows from Eqs. (53), (54) if one notices that the transformation $t\mapsto t\pm\pi/\omega$, $\mu\mapsto\exp(\mp 2\pi\eta/\omega)$ transforms the point $\boldsymbol{q}=\boldsymbol{X}(t)+\mu\boldsymbol{Y}(t)$ into $-\boldsymbol{q}\exp(\mp 2\pi\eta/\omega)$, and $s(t,\mu)$ as given by Eq. (50) into $s(t,\mu)\exp(\mp 2\pi\eta/\omega)$. Similarly, it follows from Eqs. (54), (73) that if both t' and t'' are shifted by $\pm\pi/\omega$, the function $M(t',t'')$ is multiplied by $\exp(\mp 2\pi\eta/\omega)$. Therefore, if $t_2(t_1)$ is a solution of Eq. (75), then $t_2(t_1\pm\pi/\omega)=t_2(t_1)\pm\pi/\omega$. The pair of equations

$$s_{\min}(\boldsymbol{q}\exp(\pm\pi\eta/\omega))=\exp(2\pi\eta/\omega)s_{\min}(-\boldsymbol{q}), \tag{77}$$

$$\boldsymbol{q}_s(t_1\pm\pi/\omega)=-\exp(\mp\pi\eta/\omega)\boldsymbol{q}_s(t_1) \tag{78}$$

expresses the covariance of the action function, and the location of the switching line, with respect to the similarity transformations.

We now address the problem of determining the optimal trajectories between which there occurs switching. In models whose parameter values satisfy Eq. (59), the caustic spiraling down to the unstable focus $\boldsymbol{q}=\boldsymbol{0}$ does not have cusp points lying along it. So there cannot occur an intersection of the projections $\boldsymbol{q}=\boldsymbol{q}(t)$ of the Hamiltonian trajectories $(\boldsymbol{q}(t),\boldsymbol{p}(t))$ that lie on one and the same turn of the LM [i.e., with $t_1\leqslant t<t_1+2\pi/\omega$, see Fig. 3(a)] and that have not encountered the fold [i.e., $\boldsymbol{q}(t)$ has not been reflected from the caustic]. In other words, if we describe the paths $\boldsymbol{q}(t)$ in polar coordinates as $(q(t),\Theta(t))$ [with the extended angular variable, $\Theta(t+2\pi/\omega)=\Theta(t)+2\pi$], then the paths with $\Theta_1\leqslant\Theta(t)<\Theta_1+2\pi$ and $\mu>\mu_c(t)$ cannot intersect each other for any Θ_1. However, there may (and does) occur switching between the projections of the trajectories $\boldsymbol{q}(t),\boldsymbol{p}(t)$ that lie on *different* turns, and have phases $\Theta(t)$ that differ by a multiple of 2π. As emphasized previously, the MPHP is surrounded on either side by optimal paths (see Fig. 6). It is clear from Fig. 6 that, since the MPHP spirals down to the point $\boldsymbol{q}=\boldsymbol{0}$, intersection of optimal paths, and switching, may occur only between paths that lie on opposite sides of the MPHP and differ in Θ by 2π. So the signs of μ must be opposite for crossing optimal paths, i.e., $\mu_1\mu_2<0$.

The switching line spirals down to the point $\boldsymbol{q}=\boldsymbol{0}$ along with the MPHP and the caustic (not shown in Fig. 6), and these three spirals never intersect one another. The pattern of switching we have just deduced corresponds to the form of the cross section of $s_{\min}=s_{\min}(\boldsymbol{q})$ shown in Fig. 5. Switching occurs between sections of $s=s(\boldsymbol{q})$ that correspond to neighboring turns of the LM, and, as a consequence of this switching, the gradient of $s_{\min}(\boldsymbol{q})$ is discontinuous at the switching line.

VII. OPTIMAL PATHS IN THE PRESENCE OF CUSP POINTS

Our topological approach to the analysis of extreme paths makes it possible to investigate the more complicated case when there are cusp points lying along the caustic that spiral down to the unstable focus at $\boldsymbol{q}=\boldsymbol{0}$. It follows from Eqs. (41) and (59) that this phenomenon occurs in any model whose characteristic parameters satisfy the condition

$$|a|\leqslant\eta<3|a|. \tag{79}$$

In this parameter range the velocity of the caustic, $\dot{\boldsymbol{q}}_c(t)$, periodically becomes equal to zero. According to Eq. (58)

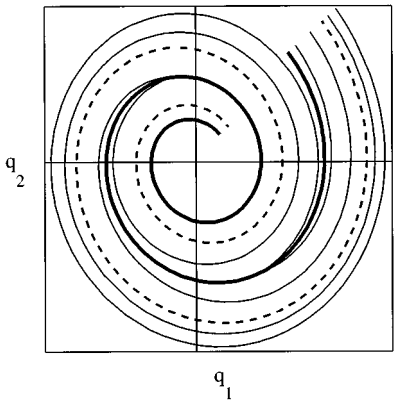

FIG. 6. Optimal paths near the unstable focus $\boldsymbol{q}=\boldsymbol{0}$, at parameter values $a=0.33$, $\omega=4.1$, and $\eta=0.45$. The MPHP is dashed, and the switching lines are solid. Between the MPHP and the nearest smaller-radius turn of the switching line lie paths with $\mu/\kappa<0$ (these paths are eventually reflected from the caustic). Paths with $\mu/\kappa>0$ lie on the opposite side of the MPHP. They cross the switching line having made one extra turn compared to the paths with $\mu/\kappa<0$, to which the system switches.

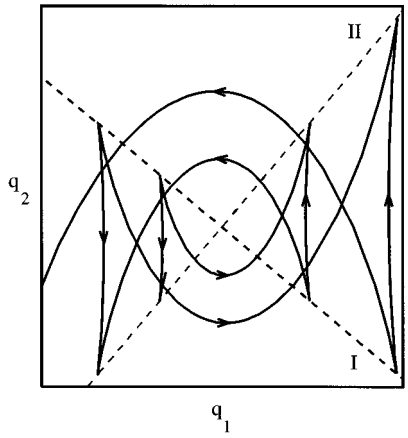

FIG. 7. The shape of the caustic spiralling down to the unstable focus $\boldsymbol{q}=\mathbf{0}$, in a model in which the caustic contains cusp points. Parameter values are the same as in Fig. 6. The caustic is self-similar, and the cusps lie on the dashed lines that pass through the focus. The numbers on the dashed lines indicate cusps of types I and II (see the text; for the parameter values chosen, the cusps are not ''observable''). Arrows indicate the direction of motion of extreme paths that are reflected from the caustic.

this happens four times per period $2\pi/\omega$, at the instants $t_n^{(1)}$ and $t_n^{(2)}$, $n=0,\pm1,\pm2,\ldots$, defined by

$$t_n^{(1)}=\frac{1}{2\omega}\arcsin\left(\frac{1+\gamma^2}{1-\gamma^2}\sin 2\Phi\right)-\frac{\phi+\Phi}{\omega}+\frac{\pi}{\omega}\left(n+\frac{1}{2}\right),$$

$$t_n^{(2)}=t_n^{(1)}+\frac{1}{\omega}\left[\frac{\pi}{2}-\arcsin\left(\frac{1+\gamma^2}{1-\gamma^2}\sin 2\Phi\right)\right]. \qquad (80)$$

Here

$$\Phi\equiv\frac{1}{2}\arctan\frac{\eta}{3\omega}.$$

The velocity of the caustic equaling zero is the sign of a cusp. It can be shown from Eqs. (31), (56) that the positions of the cusp points, $\boldsymbol{q}_c(t_n^{(i)})$, form two *self-similar sets*: they satisfy

$$\boldsymbol{q}_c(t_{n+1}^{(i)})=-\exp\left(-\frac{\eta\pi}{\omega}\right)\boldsymbol{q}_c(t_n^{(i)}),\quad i=1,2. \qquad (81)$$

The shape of the caustic, in the parameter range (79), is shown in Fig. 7. The caustic spirals down to the unstable focus at $\boldsymbol{q}=\mathbf{0}$, but now it has four cusp points per turn. As in models without cusp points along the caustic, the caustic is self-similar: it is invariant with respect to the similarity transformations $\boldsymbol{q}\mapsto-\boldsymbol{q}\exp(\mp\pi\eta/\omega)$.

A. The Lagrangian manifold

A better insight into the shape of the caustic and the flow field of extreme trajectories can be gained from an analysis of the two-dimensional Lagrangian manifold, in the four-dimensional phase space, that is traced out by the trajectories. We note that the internal part of the integral surface in Fig. 3(a) (which includes the fold) is basically the internal fold of a torus. It is known from catastrophe theory that a plane projection of the internal fold of a torus may contain cusp points [39]. A portion of a turn of the surface $p_1=p_1(\boldsymbol{q})$ in the case when cusp points are present is shown schematically in Fig. 8. The cusp points arise if the fold is bent, and makes a sufficiently small angle with the normal to the projection plane. One can picture the fold and the cusp points on it by thinking of a doughnut seen at a small angle. In contrast to the surface of a doughnut, the integral surface $p_1=p_1(\boldsymbol{q})$ [or $p_2=p_2(\boldsymbol{q})$] is not closed, but on the whole, the fold winds around the axis $\boldsymbol{q}=\mathbf{0}$. Therefore one would expect to have four cusp points per turn, as in the case of a doughnut. This is in agreement with Eqs. (31), (56), (80), which give the positions of the cusp points explicitly.

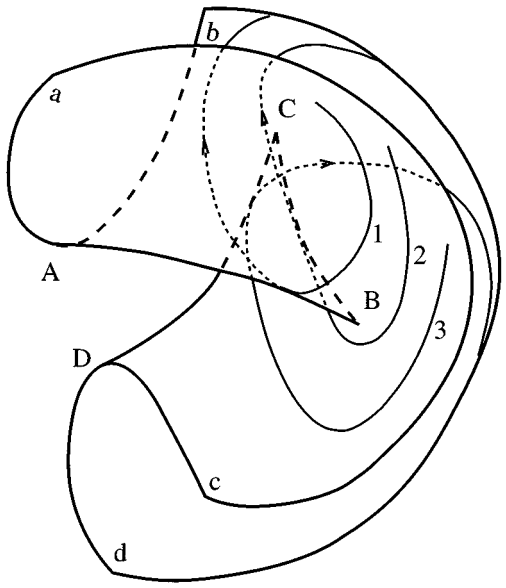

FIG. 8. A portion of the surface $p_1=p_1(\boldsymbol{q})$, showing folding. Cusp points on the caustic are the projections of points on this surface at which folds begin or end.

In Sec. III A we pointed out that cusp points should be distinguished depending on whether extreme trajectories (1) first enter the interior of the cusp and then hit the caustic, or (2) first hit the segment of the caustic that contains the cusp point, and then leave the area delimited by the caustic. We shall now establish which of these two types (types I and II, respectively) occurs at the instants $t_n^{(1)}$ and $t_n^{(2)}$ of Eq. (80).

The direction in which the two branches of the caustic extend from a cusp point is given by the vector $\ddot{\boldsymbol{q}}_c$ [cf. Fig. 1(b).] It is clear that if at a cusp point the extreme path $\boldsymbol{q}(t)$ that hits the cusp point satisfies the inequality $\ddot{\boldsymbol{q}}_c\cdot\partial\boldsymbol{q}/\partial t>0$, then this path will stay inside the region between the branches of the caustic. So if the inequality holds, the cusp will be of type I. If the opposite inequality holds, then the cusp will be of type II.

As mentioned above, at the point where an extreme path touches (and is reflected from) the caustic, the vectors $\boldsymbol{Y}(t)$ and $\dot{\boldsymbol{q}}(t)$ are antiparallel, i.e., $\boldsymbol{Y}(t)\cdot\dot{\boldsymbol{q}}(t)<0$, whereas $\boldsymbol{Y}(t)$ and $\dot{\boldsymbol{q}}_c(t)$ are parallel. Clearly, at the cusp points $\boldsymbol{Y}(t)$ and $\ddot{\boldsymbol{q}}_c(t)$ are parallel or antiparallel. Since at this point $dl/dt\equiv d(\boldsymbol{Y}\cdot\dot{\boldsymbol{q}}_c)/dt=\boldsymbol{Y}\cdot\ddot{\boldsymbol{q}}_c$, it is clear that the type of cusp point is determined by the sign of dl/dt. So we have at the cusp point

$$\mathcal{L}(t)=0, \quad \frac{dl}{dt}=\begin{cases}<0, & \text{for type I}\\ >0, & \text{for type II.}\end{cases} \tag{82}$$

It follows from Eq. (82) and from the explicit formula for $\mathcal{L}(t)$ [Eq. (58)] that the cusp points encountered at the instants $t=t_n^{(1)}$ are of type I, whereas those occurring at the instants $t=t_n^{(2)}$ are of type II. So type I and type II cusps occur alternately, two pairs per turn of the LM.

The presence of cusp points does not change qualitatively the behavior of the flow of Hamiltonian trajectories on the Lagrangian manifold, compared to what it would be in the absence of cusps. The fact that the optimal path $\boldsymbol{q}(t)=\boldsymbol{X}(t)$ (the MPHP) spirals all the way down to the unstable point $\boldsymbol{q}=\boldsymbol{0}$ does not change. (It is no longer smooth, of course.) The fact that the extreme trajectories $\boldsymbol{q}(t)=\boldsymbol{X}(t)+\mu\boldsymbol{Y}(t)$ with $\mu>0$ do not encounter the caustic also does not change. However, the projection of some of these trajectories onto the (q_1,q_2)-plane (i.e., the $\boldsymbol{p}=\boldsymbol{0}$ plane) is now qualitatively changed.

Extreme trajectories with $\mu<0$ now split into three groups, depending on which of the three branches of the caustic (two coming in and out of the pair of cusp points, and one connecting the cusp points, see Figs. 7 and 8) they hit. The corresponding three types of Hamiltonian trajectories are shown in Fig. 8. To make the description more convenient we have labeled the parts of the surface $p_1=p_1(\boldsymbol{q})$ in the following way: parts *a* and *c* are both facing upward; they coincide, except that *c* includes the ''invisible'' part of the upfacing sheet that is hidden behind the fold *AB*; parts *b* and *d* are both facing downward (''invisible'' parts of the trajectories are shown dashed). In Fig. 8, trajectory 1 comes from part *a*, and then goes over the fold *AB* to part *b* and becomes invisible. Trajectory 2 goes around the cusp point *B* from part *a* to part *c*, and then goes over the fold *BC* to part *b*. Trajectory 3 also goes around the cusp *B* to part *c* of the surface, but then it goes over the fold *DC* to part *d*.

B. Switching lines

It is clear from Fig. 8 that, in the presence of cusp points, the extreme paths $\boldsymbol{q}(t)=\boldsymbol{X}(t)+\mu\boldsymbol{Y}(t)$ with $\mu<0$ cross each other before they encounter the caustic. Therefore, one would expect to find a switching line not only between paths with $\mu<0$ and $\mu>0$, but also between different paths with $\mu<0$ (for some such paths, at least). The two types of switching compete with each other: by the time the paths with $\mu<0$ cross each other they may have become ''invisible'' because the system has switched to the paths with $\mu>0$, on account of the latter having lesser action. In this case the pattern of switching is exactly the same as that analyzed in Sec. VI, for models without cusp points on the caustic. We now consider the case when switching between the paths with $\mu<0$ is in fact observable. We shall find the parameter range where this occurs.

Insight into the possible sorts of switchings can be gained from Figs. 8, 9(a), 9(b). In Fig. 8 the paths 2 and 3 intersect after encountering the caustic. They are nonoptimal at the intersection point, so there is no switching line associated with their intersection. This corresponds to the cusp point *C* being of type II. The paths 1 and 2, on the other hand,

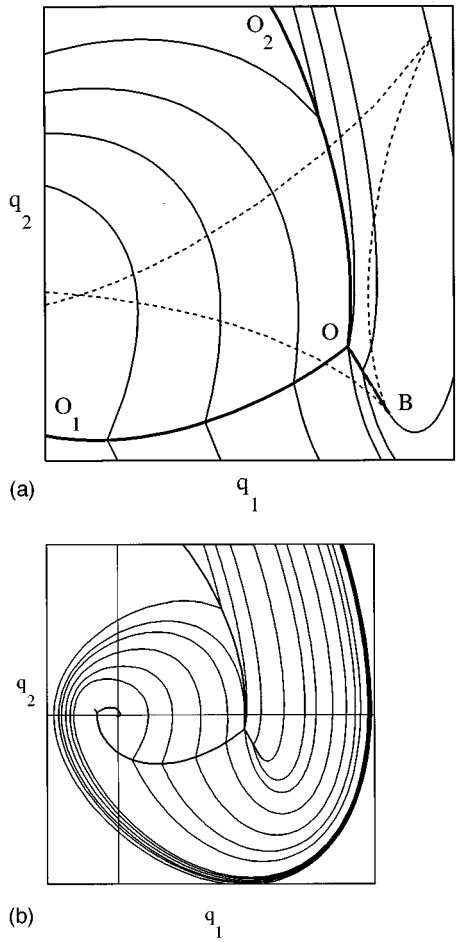

FIG. 9. A multibranched switching line (bold), in a model in which the caustic spiraling down to the unstable focus contains observable cusp points. Optimal paths that cross the switching line are shown with thin solid lines. Parameter values are $a=0.855$, $\omega=1.53$, and $\eta=0.9$. (a) The local structure of the switching line. The caustic is shown dashed. The section *BO* starts at the observable cusp point *B*. (b) A lower-resolution plot, showing the self-similar structure of optimal paths and switching lines. The switching line spirals down to the unstable focus at the origin, like the caustic. The structure close to the focus is not resolved.

intersect *before* they encounter the branches of the caustic that emanates from the type-I cusp point *B*. This cusp point may be observable. If so, there is a switching line between the trajectories 1 and 2, which emanates from the point *B*. This switching line is shown in Fig. 9(a) as the line *BO*. Clearly, the switching line lies inside the triangle formed by the caustic [where the projections of the parts *a* and *c* of the $p_1=p_1(\boldsymbol{q})$ surface on which the trajectories 1 and 2 lie, overlap].

The switching line that starts at *B* is described by the solution of Eq. (75): $t_2=t_2(t_1)$. At the cusp point $t_1=t_2=t_n^{(1)}$ and away from it, $t_1<t_n^{(1)}<t_2$. The end point *O* of the switching line is determined by the value t_1^* where Eq. (75) has two roots $t_2^{*\prime}$, $t_2^{*\prime\prime}$ such that the three optimal paths that come to the point *O* at the instants t_1^*, $t_2^{*\prime}$, $t_2^{*\prime\prime}$ have the same classical action. The third path (not shown in Fig. 8) is a path $\boldsymbol{q}(t)=\boldsymbol{X}(t)+\mu\boldsymbol{Y}(t)$ with $\mu>0$. It makes an additional turn around the unstable focus compared to the

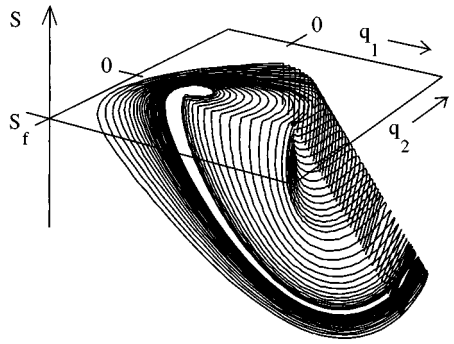

FIG. 10. The action $S=S(\boldsymbol{q})$ near the unstable focus, in a model in which the switching line is multibranched. The parameters are the same as in Fig. 9. The ''edges'' of $S(\boldsymbol{q})$ [the curves where $\nabla S(\boldsymbol{q})$ is discontinuous] project to the switching lines (cf. Fig. 9). ''Vertices'' of $S(\boldsymbol{q})$ (one is shown as a bold dot) are points at which the switching line branches.

paths of type 1 and 2. All three optimal paths terminating at O are shown in Fig. 9(b).

The intersections of the optimal paths of types 1 and 2 with the optimal paths with $\mu>0$ gives rise to the switching lines OO_1 and OO_2, respectively. At the point O the three switching lines BO, OO_1, and OO_2 intersect each other, which is an illustration of the *branching of switching lines* mentioned briefly in Sec. III A. In the present case this situation is explicitly characterized by Eqs. (73), (75), which were used to obtain Figs. 9(a) and 9(b).

The surface of minimum action $s_{\min}=s_{\min}(\boldsymbol{q})$ corresponding to the pattern of optimal paths in Figs. 9(a) and 9(b) is defined piecewise, in the regions separated by switching lines. It is continuous, but the slope $\boldsymbol{\nabla} s_{\min}(\boldsymbol{q})$ is discontinuous on the switching lines. The surface $s_{\min}=s_{\min}(\boldsymbol{q})$ has a so-called vertex at the point O. A vertex is a new generic type of singularity of the classical action. In contrast to a cusp point, the WKB prefactor in the stationary probability density is not expected to blow up at a vertex. Near O, the probability distribution is given by the well-behaved asymptotic expression

$$P(\boldsymbol{q})\sim\sum_{i=1,2,3}C_i(\boldsymbol{q})\exp[-S_i(\boldsymbol{q})/D],\quad D\to 0, \tag{83}$$

where the actions $S_i(\boldsymbol{q})$, $i=1,2,3$, arise from extreme trajectories on the three sheets of the surface of minimum action, and the coefficients C_i are the WKB prefactors for each of the sheets.

The above analysis dealt only with a single pair of cusp points. The global pattern of switching lines (i.e., of the multibranched switching line) is shown in Fig. 9(b). This multibranched line is self-similar, as is the switching line in the absence of cusps, cf. Eq. (77). The corresponding surface of minimum action $s_{\min}=s_{\min}(\boldsymbol{q})$ is shown in Fig. 10. This surface is self-similar as well, and satisfies Eq. (77). The condition for a multibranched switching line to occur is that the action at the cusp point B evaluated along the paths with $\mu>0$ be larger than that for the paths with $\mu<0$. Otherwise the extreme paths with $\mu<0$ that cross each other along the line BO in Fig. 9(a) will have ceased to be optimal paths by the time they cross. One can imagine that by varying the parameters of the dynamical system, one could force the point O in Fig. 9(a) to coincide with the point B. In this case the switching line BO would disappear, and there would remain only the smooth switching line O_1O_2. In fact, the points B and O will coincide provided

$$s(t_n^{(1)},\mu_c(t_n^{(1)}))=s(t',\mu),$$
$$\boldsymbol{X}(t_n^{(1)})+\mu_c(t_n^{(1)})\boldsymbol{Y}(t_n^{(1)})=\boldsymbol{X}(t')+\mu\boldsymbol{Y}(t'),\quad \mu>0, \tag{84}$$

$\mu_c(t)$ being given by Eq. (56). Clearly, because of the self-similarity of the switching line, Eq. (84) holds for the whole switching line, i.e., for every n.

Equation (84) gives a sufficient condition for occurrence of a multibranched switching line. A *necessary* condition is that the normalized action $s_c(t_n^{(1)})$ at the type-I cusp points be negative [otherwise there would be an extreme path with a smaller normalized action, $s=0$, which would consist of the MPHP followed by a deterministic trajectory $\boldsymbol{q}=\boldsymbol{q}^{\mathcal{D}}(t)$ Eq. (21) extending to the specified end point]. The action on the caustic $s_c(t)$ Eq. (61) has minima at $t_n^{(1)}$, and it follows from Eq. (61) that $s_c(t_n^{(1)})<0$ provided that the characteristic parameters of the model satisfy

$$\frac{\gamma^2-1}{\gamma^2+1}\left(\frac{\eta^2+9\omega^2}{\eta^2+\omega^2}\right)^{1/2}>1,\quad \text{or}\quad |a|<\eta<(8a^2-\omega^2)^{1/2}. \tag{85}$$

(We have used the explicit expression of Eq. (55) for $\tan\phi$.) It can easily be seen that $s_c(t_n^{(2)})>0$, which again agrees with the general conclusion that the cusp points of type II are unobservable.

Although the condition (85) is necessary rather than sufficient, it follows from a numerical analysis of Eq. (84) that the condition (85) provides a reasonably good estimate of the parameter range where the cusp is observable. The reason is that the paths with $\mu<0$, to which the system switches from the paths with $\mu<0$, make an extra turn around the unstable point $\boldsymbol{q}=\boldsymbol{0}$. Therefore the term $-\frac{1}{2}\boldsymbol{X}^2(t')$ in the action for these paths has an extra factor $\sim\exp(-2\pi\eta/\omega)$. In the parameter range (85), $\exp(-2\pi\eta/\omega)<\exp(-2\pi/7^{1/2})\approx 0.09$, and therefore switching to the paths with $\mu>0$ occurs comparatively far from the MPHP. This tends to make the cusp points observable.

VIII. EXTREME PATHS FOR A van der POL OSCILLATOR

A. A local analysis

As we mentioned in Sec. II, one example of a fluctuating system with a stable limit cycle is a noise-driven van der Pol oscillator. The preceding analysis of singularities of the pattern of extreme paths near an unstable focus fully applies to this model. In this subsection we consider local features of this pattern, and in Sec. VIII B we provide numerical data on the global pattern of extreme paths.

The dimensionless coordinate q_1, and the velocity q_2 of the van der Pol oscillator of Eqs. (3), (4) may be defined so that near the unstable fixed point $\boldsymbol{q}=0$ they coincide with the

canonical variables $q_1 \equiv q_1'$ and $q_2 \equiv q_2'$ of Eqs. (34) and (43). The parameters a and b in Eqs. (40), (41) that characterize the motion near $\boldsymbol{q}=\mathbf{0}$ will then satisfy

$$a=\eta, \quad b=1. \tag{86}$$

The unstable fixed point $\boldsymbol{q}=\mathbf{0}$ of the van der Pol oscillator is an unstable focus, rather than an unstable node, provided that $\eta<1$, which we assume to be the case.

In this model the pattern of extreme paths emanating from the limit cycle, when prolonged to the vicinity of the unstable focus at $\boldsymbol{q}=\mathbf{0}$, has some unusual features, due to the diffusion matrix $\hat{\boldsymbol{Q}}$ of Eq. (4) being degenerate. It turns out that extreme paths other than the MPHP can go through the point $\boldsymbol{q}=\mathbf{0}$. Indeed, if $\hat{\boldsymbol{Q}}$ is degenerate, the condition that the quadratic Hamiltonian (19) be equal to zero at $\boldsymbol{q}=\mathbf{0}$ does not require that *both* components of the momentum p_1, p_2 be equal to zero when $\boldsymbol{q}=\mathbf{0}$. In the present case, when $Q_{11}=0$ we must have $p_2=0$ at $\boldsymbol{q}=\mathbf{0}$, but p_1 may be finite.

The following analysis confirms that the MPHP is not the only extreme path that reaches the unstable focus. For characteristic parameters of the form (86), the explicit expressions (53), (54) for the MPHP $\boldsymbol{X}(t)$ (the optimal trajectory that asymptotically approaches $\boldsymbol{q}=\mathbf{0}$ as $t\to\infty$) and for the deterministic path $\boldsymbol{Y}(t)$ [which is ''mixed'' with the MPHP to yield extreme paths of the form $\boldsymbol{X}(t)+\mu\boldsymbol{Y}(t)$] become

$$\boldsymbol{X}(t) \equiv \begin{pmatrix} X_1(t) \\ X_2(t) \end{pmatrix} = \frac{\kappa e^{-\eta t}}{\cos\phi} \begin{pmatrix} \cos(\omega t-\phi)+\sin\omega t \\ \cos(\omega t+\phi)-\sin\omega t \end{pmatrix}, \tag{87}$$

$$\boldsymbol{Y}(t) \equiv \begin{pmatrix} Y_1(t) \\ Y_2(t) \end{pmatrix} = \frac{e^{\eta t}}{1+\sin\phi} \begin{pmatrix} \cos(\omega t+\phi)+\sin(\omega t+2\phi) \\ \cos(\omega t+\phi)-\sin\omega t \end{pmatrix}, \tag{88}$$

where

$$\omega=(1-\eta^2)^{1/2}, \quad \phi=\arcsin\eta. \tag{89}$$

It follows from Eqs. (87), (88) that the components $X_2(t)$ and $Y_2(t)$ become equal to zero at the same instants of time $t_n^{(P)}$, defined by the condition

$$\cos(\omega t_n^{(P)}+\phi)-\sin(\omega t_n^{(P)})=0. \tag{90}$$

This means that all extreme trajectories $\boldsymbol{q}(t)\equiv\boldsymbol{X}(t)+\mu\boldsymbol{Y}(t)$, irrespective of the value of the mixing parameter μ, cross the axis $q_2=0$ at the instants $t_n^{(P)}$. Clearly, extreme trajectories whose parameter μ equals one of the values

$$\mu_n^{(P)} \equiv -X_1(t_n^{(P)})/Y_1(t_n^{(P)}) \tag{91}$$

will pass through the point $\boldsymbol{q}=\mathbf{0}$.

On account of this crossing, in the van der Pol model the unstable fixed point $\boldsymbol{q}=\mathbf{0}$ is itself a cusp point of the flow field of extreme trajectories. Indeed, it follows from Eqs. (87), (88) that $\dot{q}_1(t_n^{(P)}) \equiv \dot{X}_1(t_n^{(P)})+\mu\dot{Y}_1(t_n^{(P)})=0$, i.e., the velocity of the paths points along the q_2 axis at the instants $t_n^{(P)}$. On the other hand, it follows from Hamilton's equations of motion (20) that the velocity component $\dot{q}_2=(\hat{\boldsymbol{d}}\boldsymbol{q})_2+p_2$ equals zero when $\boldsymbol{q}=\mathbf{0}$. Therefore $\dot{\boldsymbol{q}}=\mathbf{0}$ at $\boldsymbol{q}=\mathbf{0}$. It can be shown that the cusp at $\boldsymbol{q}=\mathbf{0}$ points along the q_2 axis.

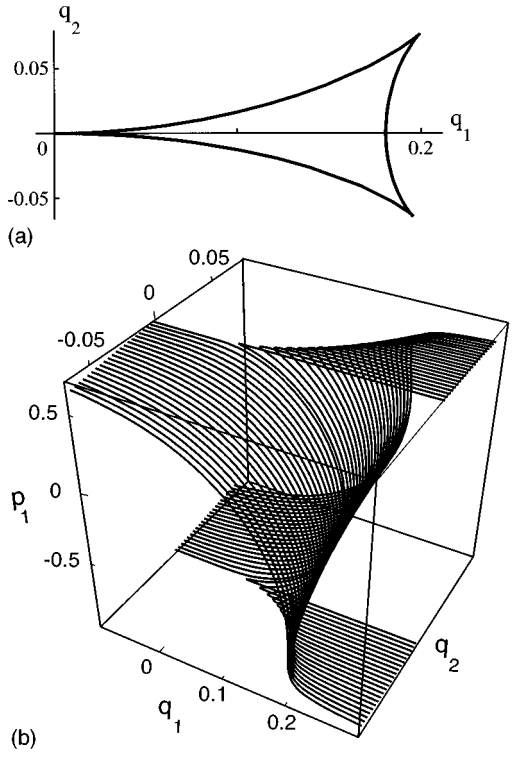

FIG. 11. (a) A portion of the surface $p_1=p_1(\boldsymbol{q})$, and (b) the corresponding section of the caustic near the unstable focus of a van der Pol oscillator. Parameter values are $a=\eta=0.45$, and $\omega=4.1$. At the focus $q_1=q_2=0$ the caustic touches the q_1 axis, and at this point the curvature of the corresponding folds of the surface $p_1(\boldsymbol{q})$ diverges.

It is straightforward to check using Eq. (56) [or, more simply, using the parametric equation (30)] that $\mu_n^{(P)}=\mu_c(t_n^{(P)})$, i.e., the point $\boldsymbol{q}=\mathbf{0}$ lies on the caustic. Since the caustic is self-similar, it passes through the point $\boldsymbol{q}=\mathbf{0}$ infinitely many times, and the caustic is parabolic near $\boldsymbol{q}=\mathbf{0}$. It follows from Eqs. (79) and (86) that, for the van der Pol oscillator, near the point $\boldsymbol{q}=\mathbf{0}$ the caustic $\boldsymbol{q}_c(t)$ has four cusp points over each period of revolution $2\pi/\omega$. When $\eta>8^{-1/2}$ half of these cusp points may be observable (i.e., physically significant), as explained in Sec. VII B.

The shape of the caustic and the shape of the surface $p_1=p_1(\boldsymbol{q})$ can be understood from Figs. 11 and 12. In Fig. 11 we show a part of the surface $p_1=p_1(\boldsymbol{q})$ and of the caustic, as generated by a half-period of revolution of the extreme paths ($\Delta t=\pi/\omega$). The general picture can be obtained from what is shown by using the similarity transformation (66) [the global shape of the caustic is seen in Fig. 12(b)]. It is clear from Fig. 11 that the caustic is tangent to the axis $q_2=0$ at $\boldsymbol{q}=\mathbf{0}$, and that the caustic has two cusp points within the time interval π/ω. Figure 11 shows also the be-

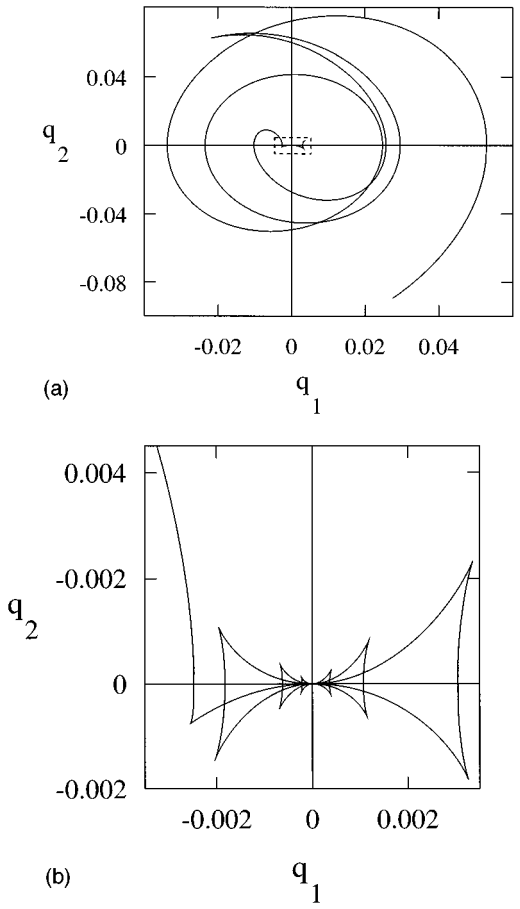

FIG. 12. The caustics of the van der Pol oscillator. The value of the single parameter, η, is 0.171. (a) A cusp point far away from the unstable focus, and the two caustics emerging from it. One of these caustics spirals down to the focus, while the other moves away from it. (b) A zoomed plot of the caustic, showing the interior of the dashed rectangle in (a). The caustic is self-similar in the vicinity of the focus and has infinitely many cusp points.

havior of the surface $p_1=p_1(\boldsymbol{q})$ in the vicinity of the cusp points, and how the surface $p_1=p_1(\boldsymbol{q})$ behaves as $\boldsymbol{q}$ moves away from the vicinity of the fixed point $\boldsymbol{q}=\boldsymbol{0}$.

B. The global structure of caustics and extreme paths

A global analysis of the pattern of extreme paths can be performed by numerically solving Hamilton's equations (10), accompanied by the initial conditions (13), (15). The results of such an analysis for the van der Pol oscillator (3), (4) are shown in Figs. 13(a)–13(c). Different extreme paths were obtained by varying ξ_n (the initial distance from the limit cycle, at a certain point along the cycle). In this way the flow field of extreme paths was built up.

A low-resolution plot is shown in Fig. 13(a). The paths begin by winding away from the cycle. We show a tube of paths that start near the cycle and approach the unstable focus enclosed by the cycle. Close to the limit cycle, this tube is extremely narrow (separate paths in the tube cannot be resolved visually). In the vicinity of the unstable focus, the width of the tube increases dramatically; the paths are ''repelled,'' and they begin to spiral away from the focus. The width of the tube increases rapidly with the number of turns. We note, however, that as the paths approach the limit cycle they are ''pressed against'' the cycle, and the tube is narrowed down again. This is in agreement with the results of Secs. VI and VII: as the paths go away from the focus they become ever closer to deterministic trajectories (the trajectories that the dynamical system would follow in the absence of noise); such trajectories asymptotically approach the limit cycle as $t\to\infty$.

It follows from the analysis of the preceding sections that, close to the unstable focus, the extreme paths display one of two types of behavior depending on which side of the MPHP they lie on (the MPHP, one recalls, is the extreme [in fact optimal] path that asymptotically approaches the focus, rather than being repelled). Paths on one side of the MPHP should spiral away from the focus after they are reflected from the caustic that asymptotically approaches the focus [cf. Fig. 2(a)]. Paths on the other side of the MPHP should be repelled by the focus, and should spiral away from it, without ever encountering the caustic. These two types of behavior are indeed seen in Figs. 13(b), 13(c). In these figures we show portions of the tube of paths in Fig. 13(a) at high resolution.

By examination, the paths shown in Fig. 13(b) form four segments of a cusped caustic that spirals into the unstable focus. These segments come together at four cusp points, so the structure of the caustic is the same as in Figs. 11(b) and 12(b). Two segments of the caustic are nearly ''vertical'' and two are nearly ''horizontal.'' The horizontal sections pass through the point $q_1=q_2=0$ [only a portion of the upper horizontal section near the upper right cusp point is seen in Fig. 13(b)]. The lower right and upper left cusp points may *in general* be observable (cf. Fig. 8 and the discussion in Sec. VII B). (For the particular parameters used in preparing Fig. 13(b), it happens that the cusps are not observable; we omit the proof.)

The paths in Fig. 13(c) are self-intersecting although they do not encounter a caustic. Their behavior is completely analogous to the generic behavior shown in Fig. 2(b).

We now discuss the global structure of caustics that is shown in Fig. 12. Caustics can be found numerically from the condition [34,35] that the Jacobian $J\equiv|\partial(q_1,q_2)/\partial(t,\mu)|$ equal zero at a time t when an extreme path encounters a caustic. Here μ is the parameter that indexes the extreme paths. As mentioned above, we choose μ to be proportional to the initial value of ξ_n, the normal distance to the limit cycle at the time we begin our numerical integration. The Jacobian can be evaluated from a set of first-order differential equations that must be integrated numerically along with Hamilton's equations for an extreme path (cf. [29,41,42]). In finding caustics numerically, we searched only for ''primary'' caustics, i.e. the caustics first encountered by extreme paths (caustics touched by extreme paths that have already encountered a caustic are of no physical interest, since the extreme paths can no longer be optimal after they have been reflected from a caustic).

It is clear from Fig. 12(a) that there are two primary caustics that start inside the limit cycle. One spirals down to the unstable focus; the other spirals away from it, and heads toward the limit cycle. It is the first caustic the occurrence of

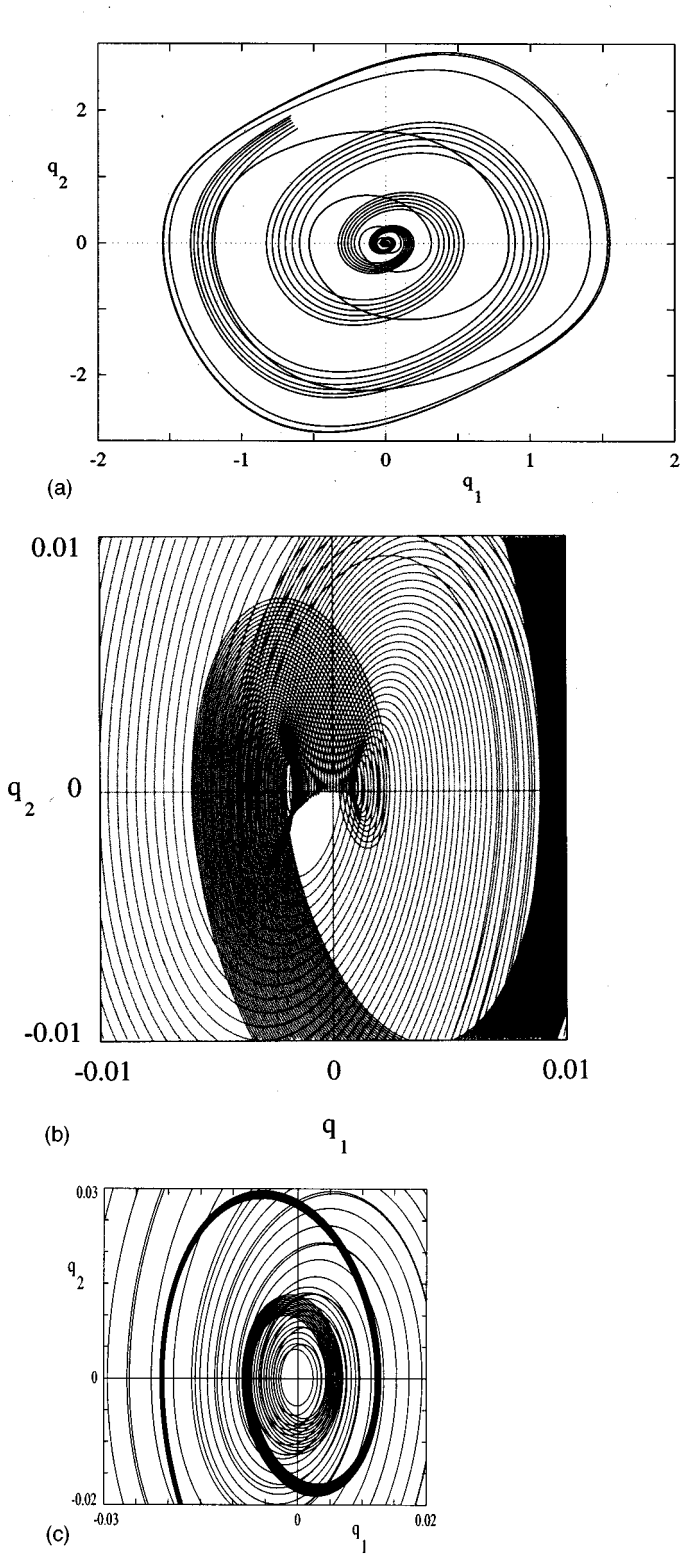

FIG. 13. Extreme paths for the van der Pol oscillator, with the same parameter value as in Fig. 12. (a) A tube of extreme paths that start near the limit cycle, initially spiral toward the unstable focus at the origin, and then spiral away from it. The tube is greatly broadened near the focus. (b) Paths that are reflected from the caustic, at points close to the focus, and then spiral back out. (c) Paths that spiral toward the focus and then spiral back out, without ever encountering the caustic.

which was predicted, and the behavior of which near the unstable focus was investigated in the present paper. In agreement with general topological expectations, the two caustics join together at a cusp point (cf. Ref. [30]). This cusp point lies away from the region near the focus where the linear approximation used in this paper applies.

The structure of the caustic near the focus is shown in Fig. 12(b). In agreement with the results of Sec. VII, the shape of the caustic is self-similar close to the focus, the caustic has four cusp points per turn, and, as a consequence of the degeneracy of the diffusion matrix, touches the focus twice per turn (cf. Fig. 11).

It is interesting to note that the infinite set of cusp points in the vicinity of the focus is separated from the cusp point from which the caustic emerges by a substantial distance, over which the caustic is smooth. We mentioned previously that observable (or potentially observable) and unobservable cusp points are encountered alternately, as one moves along the caustic. The cusp far away from the focus is obviously observable, and therefore the first cusp in the vicinity of the focus should be unobservable. This agrees with the pattern of cusp points in Fig. 13(b) discussed above.

One would like to investigate the switching line of the van der Pol model, as well as the pattern of cusps and caustics. Figure 12 provides some insight into the global structure of the switching line. We did not attempt to estimate its position numerically, but it is clear from topological arguments that it starts at the cusp point remote from the focus. It spirals smoothly down to the focus, and its behavior in the vicinity of the focus is described by the results of Sec. VII.

IX. CONCLUSIONS

The central result of the present paper is an analysis of the pattern of optimal fluctuational paths in the vicinity of an unstable focus of a periodically oscillating dynamical system. We have shown that this pattern generically displays singular behavior, and have analyzed this behavior. We have also established topological features of the *global* pattern of optimal fluctuational paths, in the interior of the limit cycle of the system.

Our approach was based on an investigation of the Lagrangian manifold $\boldsymbol{p}=\boldsymbol{p}(\boldsymbol{q})$ of an auxiliary Hamiltonian system. The classical trajectories of this system, $\boldsymbol{q}=\boldsymbol{q}(t)$, provide extrema of its action functional, whereas its zero-energy classical action $S=S(\boldsymbol{q})$ determines the exponential falloff of the stationary probability density of the original fluctuating system in the weak-noise limit. *Optimal* fluctuational paths of the original system are a special case of the zero-energy trajectories of the auxiliary system: the extreme paths of *least action*. On any such trajectory, the values taken by the spatial variables $\boldsymbol{q}$ of the auxiliary system coincide with the values taken by the dynamical variables of the original system, as it moves along an optimal fluctuational path. Additionally, the momentum variables $\boldsymbol{p}$ of the auxiliary system are related to optimal realizations of the noise $\boldsymbol{f}(t)$, which drives the dynamical system along its optimal path. Both optimal paths and optimal realizations of the noise are physically observable.

We have shown that, near an unstable focus in the space of dynamical variables of the original system ($\boldsymbol{q}=0$), the Lagrangian manifold $\boldsymbol{p}=\boldsymbol{p}(\boldsymbol{q})$ has a novel topological structure. It is many sheeted, and the surfaces $p_i=p_i(\boldsymbol{q})$, $i=1,2$, have a complicated helicoidal shape, with folds spiralling down to the focus. The projection of each fold onto the $\boldsymbol{q}$ plane is a caustic: an envelope of extreme paths, from which extreme paths are 'reflected'. Normally one associates caustics with the crossing of trajectories, but an interesting and unexpected consequence of the helicoidal structure of the surfaces $p_i=p_i(\boldsymbol{q})$ is that extreme paths on the $\boldsymbol{q}$ plane can *cross* each other, and themselves, *without* first encountering a caustic.

Generically, a caustic spirals into the unstable focus. This makes the problem qualitatively different from the problem of fluctuations in a periodically driven system, which was investigated by Graham and Tél [21]. Depending on the parameters of the system the caustic may be smooth or may have four cusp points per turn. However, caustics are not observable, in the sense that optimal paths (that is, *least-action* extreme paths) never reach them. By the time an extreme path reaches the caustic and is reflected from it, it has ceased to be optimal.

The physically observable singularities are switching lines rather than caustics. Switching lines are the curves that separate the regions in state space to which the system arrives (in the weak-noise limit) along topologically different optimal paths. We have shown that generically, a switching line spirals into the unstable focus. In the case when the caustic spiraling down to the focus has cusp points lying along it, the switching line may be multibranched: it may have segments that branch off. The minimum zero-energy action function $S_{\min}(\boldsymbol{q})$ of the associated Hamiltonian system has a singularity of a special type, a ''vertex,'' at each such branching point.

Even if there are no cusp points along the caustic spiraling down to the unstable focus, the function $S_{\min}=S_{\min}(\boldsymbol{q})$ near the unstable focus is not quadratic in the distance to the focus, except very approximately. Figure 5 makes this very clear. The cross section of $S_{\min}=S_{\min}(\boldsymbol{q})$ by a plane $a_1q_1+a_2q_2=\text{const}$ with arbitrary a_1,a_2 is the envelope of a discrete set of curves, each curve arising from a distinct branch of the multivalued function S. This envelope is a jagged approximation to a parabola, rather than being a true parabola. As a consequence of this nonquadratic behavior, the stationary probability density at points $\boldsymbol{q}$ near the focus, which includes an exponential factor $\exp[-S(\boldsymbol{q})/D]$, will in the weak-noise ($D\to 0$) limit be considerably more complicated than a straightforward inverted Gaussian.

One way of observing the novel singular features that we have derived would be to investigate the stationary probability density, or, in more depth, to measure the distribution of the fluctuational paths themselves, by using, e.g., the experimental technique of Ref. [26]. The importance of oscillating dynamical systems in physical applications would make such an analysis particularly valuable. An additional motivation for conducting such an analysis arises from the fact that, in many cases, a fluctuating system displays ''hidden'' degrees of freedom when brought to the vicinity of an unstable fixed point. This may for example happen in a laser [13]: when the intensity of the dominating mode drops down, other modes that were previously suppressed come into play, and there occurs a transient (with duration $\propto|\ln D|$, as $D\to 0$) increase in their intensity.

APPENDIX

In this appendix we provide a proof that the action computed from an extreme trajectory that has been reflected from a caustic is larger than the action computed from an extreme trajectory that has not (this statement was given without a proof in Ref. [30]). Near a caustic it is convenient to choose coordinates $\overline{q_1},\overline{q_2}$ in such a way that the unit vector $\hat{\overline{\boldsymbol{q}}}_1$ points along the caustic, and $\overline{q_2}$ is the distance to the caustic. This implies that

$$\dot{\boldsymbol{q}}=\hat{\overline{\boldsymbol{q}}}_1|\dot{\overline{\boldsymbol{q}}}|, \quad \text{at } \overline{q_2}=0.$$

As shown in Fig. 1, the coordinate $\overline{q_2}$ is quadratic in the momentum component $\overline{p_2}$ transverse to the caustic. So this momentum component, as a function of position $\boldsymbol{q}$, has two branches, i.e.,

$$\overline{p_2^{\pm}}(\overline{q_1},\overline{q_2})\approx\overline{p_2}(\overline{q_1},0)\pm[u(\overline{q_1})\overline{q_2}]^{1/2}, \quad |\overline{q_2}|\ll 1. \tag{A1}$$

The sign of u determines whether the extreme trajectories that are reflected from the caustic lie on the $\overline{q_2}>0$ side (for $u>0$) or on the $\overline{q_2}<0$ side (for $u<0$).

The action $S=S(\boldsymbol{q})$ also has two branches near the caustic. The quantity of interest is the difference between the values of S on its two sheets, at the same point $\boldsymbol{q}$. It follows from the evolution equation (11) for the action S along the Hamiltonian trajectories that $S(t)=\int\boldsymbol{p}(t)\cdot\dot{\boldsymbol{q}}(t)dt$. Therefore the difference between the values of S on the two sheets may be written as

$$S^{(+)}(\boldsymbol{q})-S^{(-)}(\boldsymbol{q})=\int_{\overline{q_2}=0}^{\overline{q_2}}\overline{p_2^{(+)}}d\overline{q_2}-\int_{\overline{q_2}=0}^{\overline{q_2}}\overline{p_2^{(-)}}d\overline{q_2}. \tag{A2}$$

It follows from Hamilton's equations (10), with account taken of (A1) and of the fact that on the caustic the transverse velocity component $\dot{\overline{q}}_2$ is zero, that near the caustic

$$\dot{\overline{q}}_2^{(\pm)}\approx\overline{Q_{22}}[\overline{p_2^{(\pm)}}(\overline{q_1},\overline{q_2})-\overline{p_2}(\overline{q_1},0)], \quad \overline{Q_{22}}\equiv\hat{\overline{\boldsymbol{q}}}_2\hat{\boldsymbol{Q}}\hat{\overline{\boldsymbol{q}}}_2. \tag{A3}$$

From this equation and the condition $\overline{Q_{22}}>0$ (the case where $\overline{Q_{22}}=0$ is nongeneric) it follows that $\operatorname{sgn}\dot{\overline{q}}_2=\operatorname{sgn}[\overline{p_2^{(\pm)}}(\overline{q_1},\overline{q_2})-\overline{p_2}(\overline{q_1},0)]$. It follows then from Eq. (A2) that the smaller action corresponds to the trajectories that *approach* the caustic (for which $\dot{\overline{q}}_2/\overline{q_2}<0$), whereas the action for the trajectories that have been reflected from the caustic is larger, at the same point $\boldsymbol{q}=(\overline{q_1},\overline{q_2})$.

In Fig. 1 therefore the sheet with the largest value of $S(\boldsymbol{q})$ is formed by paths that have been ''reflected'' by one of the caustics (these paths lie in the middle sheet of the LM). The physical value of $S(\boldsymbol{q})$, i.e., $S_{\min}(\boldsymbol{q})$, must be attained on one of the other two sheets.

[1] (a) A. A. Andronov and C. E. Chaikin, *Theory of Oscillators* (Princeton University Press, Princeton, 1949); (b) J. Guckenheimer and P. Holmes, *Nonlinear Oscillators, Dynamical Systems and Bifurcations of Vector Fields* (Springer-Verlag, New York, 1983).

[2] M. Sargent III, M. O. Scully, W. E. Lamb, Jr., *Laser Physics* (Addison-Wesley, Reading, MA, 1974); A. E. Siegman, *Lasers* (University Science Books, Mill Valley, CA, 1986).

[3] (a) I. R. Epstein, J. Phys. Chem. **88**, 187 (1984); (b) L. Edelstein-Keshet, *Mathematical Models in Biology* (Random House, New York, 1988).

[4] C. Bracikowski and R. Roy, Chaos **1**, 49 (1990).

[5] D. G. Luchinsky, A. L. Velikovich, G. P. Golubev, and V. P. Golubchenko, Opt. Commun. **80**, 444 (1991); P. La Penna and G. Giusfredi, Phys. Rev. A **48**, 2299 (1993); C. Balconi, F. Casagrande, L. A. Lugiato, W. Lange, H. Walther, Opt. Commun. **114**, 425 (1995).

[6] A. K. Bajaj, in *Dynamical Systems Approaches to Nonlinear Problems in Systems and Circuits*, edited by F. M. A. Salam (SIAM, Philadelphia, 1988); A. H. Nayfeh, S. A. Nayfeh, T. A. Anderson, and B. Balachandran, in *Nonlinearity and Chaos in Engineering Dynamics*, edited by J. M. T. Thompson and S. R. Bishop (Wiley, New York, 1994), p. 39; W. F. Langford and K. Zhan, *ibid.*, p. 241.

[7] (a) S. M. Rytov, Zh. Éksp. Teor. Phys. **29**, 304 (1955) [Sov. Phys. JETP **2**, 217 (1955)]; (b) M. Lax, in *Statistical Physics, Phase Transitions and Superconductivity*, edited by M. Chrétien, E. P. Gross, and S. Deser (Gordon and Breach, New York, 1968).

[8] A. D. Nazarea and G. Nicolis, Mol. Phys. **29**, 1557 (1975); G. Nicolis and J. W. Turner, Physica A **89**, 326 (1977); G. Nicolis and M. Malek-Mansour, Prog. Theor. Phys. Suppl. **64**, 249 (1978); A. Fraikin and H. Lemarchand, J. Stat. Phys. **41**, 531 (1985).

[9] M. I. Dykman, X. Chu, and J. Ross, Phys. Rev. E **48**, 1646 (1993).

[10] H. Haken, Phys. Rev. Lett. **13**, 329 (1964); H. Risken, Z. Phys. **186**, 85 (1965); R. Graham, *Quantum Statistics in Optics and Solid-State Physics* (Springer-Verlag, New York, 1973).

[11] R. Roy, R. Short, J. Durin, and L. Mandel, Phys. Rev. Lett. **45**, 1486 (1980).

[12] B. McNamara, K. Wiesenfield, and R. Roy, Phys. Rev. Lett. **60**, 2626 (1988).

[13] (a) M. Ohtsu, Y. Teramachi, Y. Otsuka, and A. Osaki, IEEE J. Quantum Electron. **QE-22**, 535 (1986); (b) M. Ohtsu and Y. Teramachi, IEEE J. Quantum Electron. **QE-25**, 31 (1989); M. Ohtsu, *Coherent Quantum Optics and Technology* (Kluwer Academic, Dordrecht, 1992).

[14] G. Raithel, O. Benson, and H. Walther, Phys. Rev. Lett. **75**, 3446 (1995).

[15] R. A. Linke *et al.*, IEEE J. Lightwave Technol. **LT-3**, 706 (1985); K. Y. Liou *et al.*, *ibid.* **7**, 632 (1989).

[16] A. D. Wentzell and M. I. Freidlin, Russ. Math. Surveys **25**(1) (1970); M. I. Freidlin and A. D. Wentzell, *Random Perturbations of Dynamical Systems* (Springer-Verlag, New York, 1984).

[17] R. Graham, in *Noise in Nonlinear Dynamical Systems*, edited by F. Moss and P. V. E. McClintock (Cambridge University Press, Cambridge, 1989).

[18] D. Ludwig, SIAM Rev. **17**, 605 (1975).

[19] B. J. Matkowsky and Z. Schuss, SIAM J. Appl. Math. **33**, 365 (1977); **35**, 604 (1979); B. J. Matkowsky and Z. Schuss, Phys. Lett. A **95**, 213 (1983); E. Ben-Jacob, D. J. Bergman, B. J. Matkowsky, and Z. Schuss, Phys. Rev. A **26**, 2805 (1982).

[20] M. I. Dykman and M. A. Krivoglaz, Sov. Phys. JETP **50**, 30 (1979).

[21] (a) R. Graham and T. Tél, Phys. Rev. Lett. **52**, 9 (1984); J. Stat. Phys. **35**, 729 (1984); (b) Phys. Rev. A **31**, 1109 (1985).

[22] (a) H. R. Jauslin, J. Stat. Phys. **42**, 573 (1986); (b) Physica A **144**, 179 (1987).

[23] (a) M. V. Day, Stochastics **20**, 121 (1987); (b) R. L. Kautz, Phys. Rev. A **38**, 2066 (1988); M. V. Day, Ann. Prob. **20**, 1385 (1992); M. V. Day, Appl. Math. Optim. **30**, 79 (1994).

[24] (a) K. Lindenberg, B. J. West, and G. P. Tsironis, Rev. Solid State Sci. **3**, 143 (1989), and references therein on fluctuations induced by colored noise; (b) M. I. Dykman, Phys. Rev. A **42**, 2020 (1990); (c) S. J. B. Einchcomb and A. J. McKane, Phys. Rev. E **51**, 2974 (1995).

[25] T. Naeh, M. M. Kłosek, B. J. Matkowsky, and Z. Schuss, SIAM J. Appl. Math. **50**, 595 (1990).

[26] M. I. Dykman, P. V. E. McClintock, V. N. Smelyanskiy, N. D. Stein, and N. G. Stocks, Phys. Rev. Lett. **68**, 2718 (1992).

[27] V. A. Chinarov, M. I. Dykman, and V. N. Smelyanskiy, Phys. Rev. E **47**, 2448 (1993).

[28] R. S. Maier and D. L. Stein, Phys. Rev. Lett. **69**, 3691 (1992).

[29] R. S. Maier and D. L. Stein, Phys. Rev. Lett. **71**, 1783 (1993); R. S. Maier and D. L. Stein, Phys. Rev. E **48**, 931 (1993).

[30] M. I. Dykman, M. M. Millonas, and V. N. Smelyanskiy, Phys. Lett. A **195**, 53 (1994).

[31] D. Leonard and L. E. Reichl, J. Chem. Phys. **92**, 6004 (1990); M. I. Dykman, E. Mori, J. Ross, and P. M. Hunt, J. Chem. Phys. **100**, 5735 (1994).

[32] M. M. Millonas and L. E. Reichl, Phys. Rev. Lett. **68**, 3125 (1992); S. Kim and L. E. Reichl, Phys. Rev. E **49**, 3088 (1996).

[33] L. Onsager and S. Machlup, Phys. Rev. **91**, 1505 (1953); **91**, 1512 (1953).

[34] M. V. Berry, Adv. Phys. **35**, 1 (1976); L. S. Schulman, *Techniques and Applications of Path Integration* (Wiley, New York, 1981); V. P. Maslov and M. V. Fedoriuk, *Semi-Classical Approximation in Quantum Mechanics* (Reidel, Boston, 1981).

[35] A. M. Anile, J. K. Hunter, P. Pantano, and G. Russo, *Ray Methods for Nonlinear Waves in Fluids and Plasmas* (Longman, New York, 1993).

[36] R. Kubo, K. Matsuo, and K. Kitahara, J. Stat. Phys. **51**, 9 (1973); R. Graham, in *Coherence and Quantum Optics*, edited by L. Mandel and E. Wolf (Plenum, New York, 1973).

[37] L. D. Landau and E. M. Lifshitz, *Mechanics* (Pergamon, London, 1976).

[38] R. P. Feynman and A. R. Hibbs, *Quantum Mechanics and Path Integrals* (McGraw-Hill, New York, 1965).

[39] H. Whitney, Ann. Math. **62**, 374 (1955); V. I. Arnold, *Catastrophe Theory* (Springer-Verlag, New York, 1984).

[40] V. I. Arnold, *Mathematical Methods of Classical Mechanics* (Springer-Verlag, New York, 1978).

[41] R. S. Maier and D. L. Stein, J. Stat. Phys. **83**, 291 (1996).

[42] R. S. Maier and D. L. Stein, SIAM J. Appl. Math. (to be published).